UNIVERSITY OF COPENHAGEN



Københavns Universitet

Phytoalexins of the crucifer Barbarea vulgaris

Structural profile and correlation with glucosinolate turnover

Cárdenas, Pablo D.; Landtved, Jonas P.; Larsen, Signe H.; Lindegaard, Nicolai; Wøhlk, Sebastian; Jensen, Karen R.; Pattison, David I.; Burow, Meike; Bak, Søren; Crocoll, Christoph; Agerbirk, Niels

Published in:
Phytochemistry

DOI:
10.1016/j.phytochem.2023.113742

Publication date:
2023

Document version
Publisher's PDF, also known as Version of record

Document license:
CC BY

Citation for published version (APA):
Cárdenas, P. D., Landtved, J. P., Larsen, S. H., Lindegaard, N., Wøhlk, S., Jensen, K. R., Pattison, D. I., Burow, M., Bak, S., Crocoll, C., & Agerbirk, N. (2023). Phytoalexins of the crucifer Barbarea vulgaris: Structural profile and correlation with glucosinolate turnover. *Phytochemistry*, *213*, Article 113742. https://doi.org/10.1016/j.phytochem.2023.113742

Download date: 20. Aug. 2026

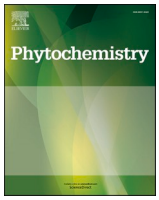
Phytochemistry 213 (2023) 113742



Contents lists available at ScienceDirect

Phytochemistry

journal homepage: www.elsevier.com/locate/phytochem





Phytoalexins of the crucifer *Barbarea vulgaris*: Structural profile and correlation with glucosinolate turnover

Pablo D. Cárdenas, Jonas P. Landtved [1], Signe H. Larsen [1], Nicolai Lindegaard [1], Sebastian Wøhlk [1], Karen R. Jensen, David I. Pattison, Meike Burow, Søren Bak, Christoph Crocoll, Niels Agerbirk [*]

Department of Plant and Environmental Sciences, University of Copenhagen, Thorvaldsensvej 40, 1871, Frederiksberg C, Denmark

ARTICLE INFO

Keywords:
Phytoalexin biosynthesis
Glucosinolate hydrolysis
Myrosinase
2-Phenylethylglucosinolate
Gluconasturtiin
Indole glucosinolates
Indole phytoalexins
Benzenic glucosinolates
Aromatic glucosinolates
Copper chloride
Elicitation
Induction
Brassicaceae
Tribe cardamineae

ABSTRACT

Phytoalexins are antimicrobial plant metabolites elicited by microbial attack or abiotic stress. We investigated phytoalexin profiles after foliar abiotic elicitation in the crucifer *Barbarea vulgaris* and interactions with the glucosinolate-myrosinase system. The treatment for abiotic elicitation was a foliar spray with $CuCl_2$ solution, a usual eliciting agent, and three independent experiments were carried out. Two genotypes of *B. vulgaris* (G-type and P-type) accumulated the same three major phytoalexins in rosette leaves after treatment: phenyl-containing nasturlexin D and indole-containing cyclonasturlexin and cyclobrassinin. Phytoalexin levels were investigated daily by UHPLC-QToF MS and tended to differ among plant types and individual phytoalexins. In roots, phytoalexins were low or not detected.

In treated leaves, typical total phytoalexin levels were in the range 1–10 nmol/g fresh wt. during three days after treatment while typical total glucosinolate (GSL) levels were three orders of magnitude higher. Levels of some minor GSLs responded to the treatment: phenethylGSL (PE) and 4-substituted indole GSLs. Levels of PE, a suggested nasturlexin D precursor, were lower in treated plants than controls. Another suggested precursor GSL, 3-hydroxyPE, was not detected, suggesting PE hydrolysis to be a key biosynthetic step. Levels of 4-substituted indole GSLs differed markedly between treated and control plants in most experiments, but not in a consistent way.

The dominant GSLs, glucobarbarins, are not believed to be phytoalexin precursors. We observed statistically significant linear correlations between total major phytoalexins and the glucobarbarin products barbarin and resedine, suggesting that GSL turnover for phytoalexin biosynthesis was unspecific. In contrast, we did not find correlations between total major phytoalexins and raphanusamic acid or total glucobarbarins and barbarin.

In conclusion, two groups of phytoalexins were detected in *B. vulgaris*, apparently derived from the GSLs PE and indol-3-ylmethylGSL. Phytoalexin biosynthesis was accompanied by depletion of the precursor PE and by turnover of major non-precursor GSLs to resedine. This work paves the way for identifying and characterizing genes and enzymes in the biosyntheses of phytoalexins and resedine.

1. Introduction

Phytoalexins are antimicrobial metabolites elicited by (*i.e.* biosynthesized *de novo* in response to) microbial attack of plants and certain abiotic stresses (VanEtten et al., 1994; Pedras et al., 2011). Phytoalexins are of considerable interest as they exhibit diverse chemical structures and bioactivities that are finding use in plant breeding for disease resistance (Pedras et al., 2011; Ahuja et al., 2012; Møldrup et al., 2013; Ahmed and Kovinich, 2021; Kariya et al., 2023). Both UV-radiation and heavy metal salts, e.g., $CuCl_2$, are abiotic stresses reported to elicit phytoalexin biosynthesis and routine screening for phytoalexins often uses abiotic stresses (Pedras et al., 2011). One reason for experimental use of abiotic rather than biotic elicitation is that many fungal pathogens metabolize and detoxify phytoalexins, generating additional metabolites that are not phytoalexins (Pedras and Abdoli, 2017).

Phytoalexins in the Brassicales order usually contain sulfur in an

* Corresponding author.
E-mail address: nia@plen.ku.dk (N. Agerbirk).
[1] These authors contributed equally to this study and are listed in alphabetical order.

https://doi.org/10.1016/j.phytochem.2023.113742
Received 30 March 2023; Received in revised form 25 May 2023; Accepted 28 May 2023
Available online 1 June 2023
0031-9422/© 2023 The Authors. Published by Elsevier Ltd. This is an open access article under the CC BY license (http://creativecommons.org/licenses/by/4.0/).

N–C–S motive, and this structural motif suggested a biosynthetic relationship to glucosinolates (GSLs) and isothiocyanates (Monde et al., 1994; Pedras et al., 2011; Pedras and Abdoli, 2017; Plaszkó et al., 2022). The GSLs are sulfur-containing metabolites in plants of the Brassicales order, capable of transformation to isothiocyanates (Halkier, 2016; Barco and Clay, 2019; Blažević et al., 2020). Isothiocyanates formed by hydrolysis of preexisting GSLs are by definition not phytoalexins (VanEtten et al., 1994). The GSLs are generally constitutive metabolites although levels are subject to complex regulation (e.g. Jeschke et al., 2019; Malhotra et al., 2022). *De novo* biosynthesis of Brassicales phytoalexins from GSLs via isothiocyanates has been demonstrated in several cases by labelling studies (e.g. Pedras et al., 2011; Pedras and Yaya, 2013; Pedras and To, 2018) but is not universal (Schuhegger et al., 2007; Møldrup et al., 2013; Mucha et al., 2019). In one case, the phytoalexin brassinin (**P1**), genes and enzymes involved in biosynthesis via isothiocyanate were discovered in the crop *Brassica rapa* L. (Fig. 1). The biosynthesis showed a remarkable overall similarity to GSL biosynthesis concerning the kinds of reactions and enzymes involved (Klein and Sattely, 2015, 2017).

Many phytoalexins in crucifers contain an indole moiety and several are derived from indol-3-ylmethylGSL (IM) (Pedras and Yaya, 2013). They can be termed "indole phytoalexins" in analogy with the term "indole GSLs" commonly used for IM and derivatives. Three indole phytoalexins are discussed in this paper and numbered **P1**, **P2** and **P3** (Fig. 1). Brassinin (**P1**) is a representative example of an indole phytoalexin and a biosynthetic precursor of several derivatives, including cyclobrassinin (**P2**) (Fig. 1) (Pedras, 2014). The CYP71CR2 enzyme from *B. rapa* was suggested to catalyze the cyclization of **P1** to **P2** (Klein and Sattely, 2017). In *Nasturtium officinale* W.T. Aiton (watercress), a cyclobrassinin isomer with the sulfur atom of the thiocarbonyl group linked to C-4 of the indole moiety was named cyclonasturlexin (**P3**) (Pedras and To, 2016) (Fig. 1). Administration of isotopically labelled precursors to *N. officinale* demonstrated that **P1** is a precursor of **P3**, but the enzymology of the conversion is yet unknown (Pedras and To, 2016).

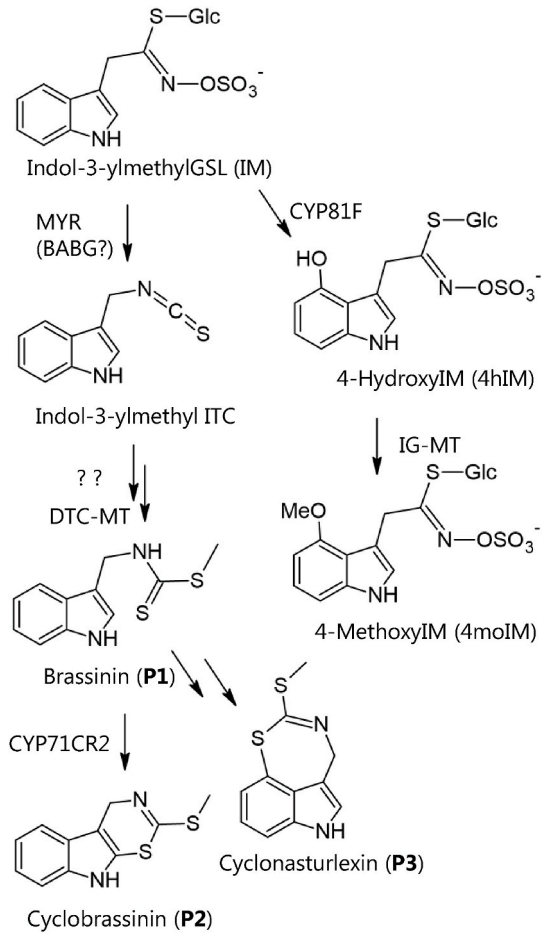


Fig. 1. Suggested biosynthesis of cyclobrassinin (**P2**) and cyclonasturlexin (**P3**), indole phytoalexins detected in *Barbarea vulgaris*, and the branching biosynthetic pathway of 4-substituted indole glucosinolates. GSL, glucosinolate; ITC, isothiocyanate; MYR, unspecified myrosinase; BABG, suggested myrosinase catalyzing hydrolysis in intact tissue upon phytoalexin elicitation; DTC-MT, dithiocarbamate methyltransferase; CYP71CR2, cytochrome P450 71CR2; CYP81F, cytochrome P450 81F; IG-MT indole GSL methyl transferase.

The finding of GSLs and isothiocyanates to be also precursors in *de novo* biosynthesis of phytoalexins attracts attention to the control of GSL hydrolysis and fates of isothiocyanates. Dedicated thioglucosidase enzymes known as myrosinases are responsible for hydrolysis of the *S*-glucoside bond in GSLs, which generally happens upon tissue disruption but may also happen in intact tissue (Pastorczyk and Bednarek, 2016; Bhat and Vyas, 2019; Sugiyama et al., 2021; Lv et al., 2022). The term myrosinase (EC 3.2.1.147) is defined functionally and several subclades of glycosidase enzymes are myrosinases (Nakano et al., 2017; Blažević et al., 2020; Yamada et al., 2020; Lv et al., 2022). Enzymes from the BABG subclade of glycosidase enzymes were suggested to be responsible for conversion of IM to the corresponding isothiocyanate and downstream phytoalexins (Klein and Sattely, 2017) (Fig. 1).

Until 2015, all known crucifer phytoalexins were indole phytoalexins. In *N. officinale*, however, three "non-indole" phenyl-containing phytoalexins were discovered after $CuCl_2$ elicitation: nasturlexin A (**P4**), nasturlexin B (**P9**) and tridentatol C (**P10**) (Pedras and To, 2015) (Fig. 2). Subsequently, two related wild species, *Barbarea vulgaris* W.T. Aiton and *Barbarea verna* (Mill.) Asch. were reported to contain additional phenyl-containing phytoalexins, nasturlexins C (**P5**) and D (**P6**) and their sulfoxides **P7** and **P8** (Pedras et al., 2015). All these phenyl-containing phytoalexins showed promising bioactivities against some crucifer pathogens (Pedras and To, 2015; Pedras et al., 2015). The phenyl-containing phytoalexins discussed in this paper are arranged and numbered **P4**–**P10** (Fig. 2) according to available biosynthetic evidence as summarized below.

Biosynthesis of phenyl-containing phytoalexins was investigated in *B. verna* and *N. officinale* using tailor-made labelled precursors (Pedras and To, 2018). This systematic screen of potential precursors of nasturlexin D (**P6**) (Pedras and To, 2018) ruled out several possibilities but showed two GSLs and their corresponding isothiocyanates to be potential precursors of **P6**: phenethylGSL (PE) and 3-hydroxyphenethylGSL (3hPE) as well as the corresponding isothiocyanates (Fig. 2). Hence, also in this case, phytoalexin biosynthesis would seem to involve GSL activation. Several related phytoalexins could also be converted to **P6**, and it could not be concluded at what step the characteristic *meta*-hydroxy group was introduced (Fig. 2) (Pedras and To, 2018). Glucobarbarins were suggested not to be precursors (Pedras and To, 2018).

The initial publication of phenyl-containing phytoalexins in *B. vulgaris* and *B. verna* (Pedras et al., 2015) did not include any data on potential indole phytoalexins in the genus. For this reason, it was relevant to investigate the profile of both indole phytoalexins and phenyl-containing phytoalexins, preferably in genotypes well suited for future genetic investigations. Two genotypes of *B. vulgaris*, known as the G- and P-types, are genetically well characterized (Kuzina et al., 2011; Liu et al., 2016, 2019a; Byrne et al., 2017). As the ecological biochemistry and GSL profiles of the two genotypes contrast with each other (Liu et al., 2016, 2019b; Erthmann et al., 2018; Günther et al., 2022), it was of interest to compare their phytoalexin profiles and biosynthesis.

The GSLs in *B. vulgaris* are all potential substrates of myrosinase activated during phytoalexin elicitation, and some are potential direct precursors of phytoalexins. They are all structurally related to either indole phytoalexins or phenyl-containing phytoalexins, with some structural variation among the G- and P-types. Within the phenyl-containing GSLs, the pattern of substitution strongly affects the kind of product formed after myrosinase-catalyzed hydrolysis (Fig. 3). In leaves

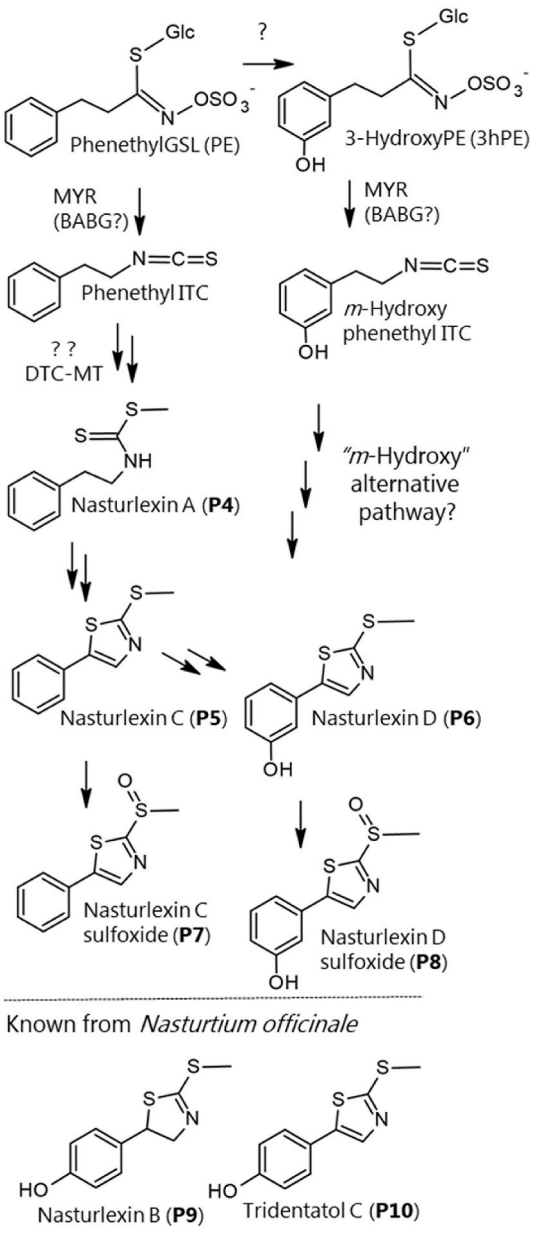


Fig. 2. Two suggested biosynthetic routes to nasturlexin D (**P6**), a phenyl-containing phytoalexin detected in *Barbarea vulgaris*. More potential intermediates are known, and more metabolic connections from the left hand side pathway to the *m*-hydroxy pathway are possible (Pedras and To, 2018). Abbreviations PE, phenethylGSL; 3hPE, 3-hydroxyPE; other abbreviations as in Fig. 1.

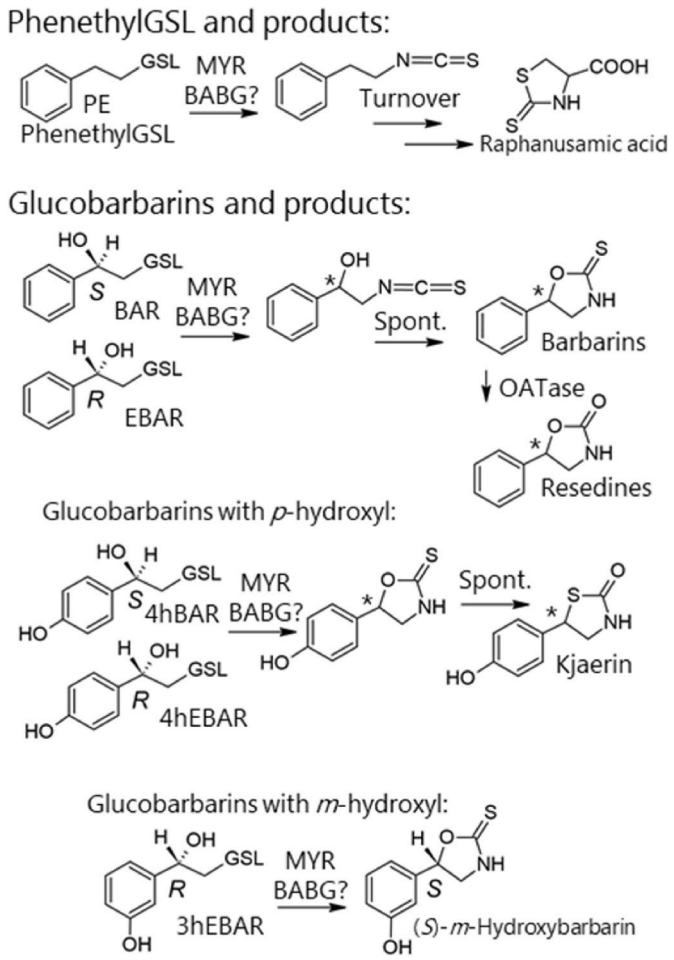


Fig. 3. Phenyl-containing glucosinolates (GSLs) in *Barbarea vulgaris* and products of their turnover catalyzed by unspecified myrosinase (MYR) or possibly BABG myrosinase upon phytoalexin elicitation. Abbreviations: PE, phenylethylGSL; BAR, glucobarbarin; EBAR, epiglucobarbarin; 4hBAR, 4-hydroxyBAR; 4hEBAR, 4-hydroxyEBAR, 3hEBAR, 3-hydroxyEBAR; OATase, oxazolidine-2-thionase; Spont., spontaneous. An asterisk indicates each illustrated, unspecified chiral center.

of both types of *B. vulgaris*, PE is mainly converted to an epimeric pair of 2-hydroxy derivatives, known by their trivial names as glucobarbarin (BAR) and epiglucobarbarin (EBAR), but low levels of remaining PE are also present in leaves (Agerbirk et al., 2015). The G-type is dominated by BAR while the P-type is dominated by EBAR. Accumulation of phenolic phenyl-containing GSLs is only known for the P-type (Agerbirk and Olsen, 2015). The main hydroxyphenyl derivative is usually 4-hydroxyepiglucobarbarin (4hEBAR) accompanied by low levels of 3-hydroxyepiglucobarbarin (3hEBAR) and 4-hydroxyphenethylGSL (4hPE). From a rare genotype collected in the Caucasus with lowered extent of 2-hydroxylation, *m*-substituted 3hPE has also been reported once (Agerbirk et al., 2015). Considering the scarcity of 3hPE in previous literature, the observation of synthetic 3hPE being an efficient precursor of the *m*-substituted phytoalexin nasturlexin D (**P6**) (Pedras and To, 2018) was unexpected.

As a basis for future elucidation of phytoalexin biosynthesis, we aimed to identify a plant organ exhibiting phytoalexin accumulation (and possibly biosynthesis) and to characterize the metabolite levels during phytoalexin elicitation in the two genotypes of *Barbarea vulgaris*. For the elicitation process, we decided to study specifically elicitation with a spray of a 10 mM $CuCl_2$ aqueous solution, as previously done (Pedras et al., 2015; Pedras and To, 2016, 2018), although 2 mM $CuCl_2$ had also been used (Pedras and To, 2015). We followed levels of potential GSL precursors of phytoalexins over time in an attempt to identify the actual precursors, and we followed levels of general GSL products as a measure of general GSL activation during phytoalexin elicitation. As a control for any observed correlations with GSLs or products, it was relevant to include metabolites not expected to be biochemically related to phytoalexins. Previous authors had tested flavonoid levels in metabolic studies of phytoalexin elicitation in *Brassica rapa* L. (Pedras et al., 2008), so we carried out a similar experiment with *B. vulgaris*. The same previous authors had likewise observed drastically increased levels of a 4-substituted indole GSL in treated plants; we also tested for that relationship in *B. vulgaris*.

Specifically, we asked the following questions: (1) Are indole phytoalexins and phenyl-containing phytoalexins elicited in roots or leaves

by a spray of 10 mM aq. $CuCl_2$ in the two types of *B. vulgaris*, what is the time-course of elicitation, and do the genotypes differ in response? (2) Are potential precursor GSLs present at the site of phytoalexin accumulation, and are levels affected? (3) Is relevant decoration of GSLs or their products affected by phytoalexin elicitation, in particular 4-substitution of indole GSLs or *m*-hydroxylation of phenyl-containing GSLs? (4) Are levels of general GSL hydrolysis products affected by phytoalexin elicitation? As a control experiment, we also investigated whether flavonoid levels were affected during elicitation of phytoalexins, as they were not considered biochemically related to phytoalexins.

2. Results

2.1. Hot extraction allowed UHPLC-QToF MS detection and quantification of phytoalexins, glucosinolates and their products, and flavonoids

Attempting to include both phytoalexins, GSLs and GSL products in a single extraction, we tested extraction in boiling MeOH–H_2O (7:3), the preferred extraction solvent for GSLs and *in vivo* GSL products in *B. vulgaris*. In initial optimization of extraction, room temperature versus hot MeOH–H_2O (7:3) solvent were compared; hot solvent systematically gave higher apparent phytoalexin levels at our conditions (165–325% of room temp. control) so we adopted hot extraction. Half of the extract was set aside for GSL analysis (Section 4.6.). For the other half of the extract, the solvent was evaporated and the residue dissolved in a solvent with lower MeOH content, MeOH–H_2O (3:7), to facilitate subsequent chromatography.

We developed a UHPLC-QToF MS method allowing separation of a wide range of flavonoids, GSL hydrolysis products and phytoalexins in one run (Table 1, Fig. 4). By a combination of *m/z* value and retention time, it was possible to distinguish all the tested phytoalexins and most GSL hydrolysis products, however, one pair of isomeric GSL hydrolysis products co-eluted (Table 1). The first minutes of the sample-chromatograms contained numerous unidentified peaks (in particular an intense peak at 2–2.2 min from *m/z* 267 and 249), peaks of known GSLs, peaks of known and putative flavonoids, and a peak of raphanusamic acid. At a retention time of 4 min or more, the phytoalexins and GSL hydrolysis products which are the focus of this investigation eluted as sharp, well separated peaks (Fig. 4B).

Table 1
Chromatographic parameters for *B. vulgaris* metabolites detected at the UHPLC-QToF MS conditions used for phytoalexin determination.

Metabolite (sum formula of M)	Authentic standard	*m/z*[a] $[M+H]^+$	t_R[b] (min)	Slope[c] (nM^{-1})	Range (μM) with detection and linearity confirmed[d]	
					Lower	Upper
Phytoalexins						
Brassinin (**P1**) ($C_{11}H_{12}N_2S_2$)	Yes	237.0515	7.4	246	0.02	0.08
Brassinin (**P1**) fragment (C_9H_7N)	Yes	130.0651	7.4	1002	0.01	10
Cyclobrassinin (**P2**) ($C_{11}H_{10}N_2S_2$)	Yes	**235.0358**	8.6	620	0.01	10
Cyclonasturlexin (**P3**) ($C_{11}H_{10}N_2S_2$)	Yes	**235.0358**	8.1	1139	0.01	10
Nasturlexin A (**P4**) ($C_{10}H_{13}NS_2$)	Yes	212.0562	8.2	754	0.01	0.16
Nasturlexin C (**P5**) ($C_{10}H_9NS_2$)	Yes	208.0249	8.8	1014	0.01	10
Nasturlexin D (**P6**) ($C_{10}H_9NOS_2$)	Yes	**224.0198**	6.6	2111	0.01	10
Putative nasturlexin C sulfoxide (**P7**) ($C_{10}H_9NOS_2$)	No	**224.0198**	5.2	(Nasturlexin D)	n.t.	n.t.
Putative nasturlexin D sulfoxide (**P8**) ($C_{10}H_9NO_2S_2$)	No	240.0147	4.7	(Nasturlexin D)	n.t.	n.t.
Nasturlexin B (**P9**) ($C_{10}H_{11}NOS_2$)	Yes	226.0355	5.5	1560	0.01	10
Tridentatol C (**P10**) ($C_{10}H_9NOS_2$)	Yes	**224.0198**	6.4	1542	0.01	10
Glucosinolate hydrolysis products and down-stream non-phytoalexin metabolites						
Barbarin (C_9H_9NOS)	Yes	180.0478	5.1	36.4	0.5	135
Resedine ($C_9H_9NO_2$)	Yes	164.0706	4.4	(Barbarin)	(0.5)	(570)
Raphanusamic acid ($C_4H_5NO_2S_2$)	Yes	163.9834	1.9–2.3	9.81	0.5	10 (25)
m-Hydroxybarbarin ($C_9H_9NO_2S$)	**Yes**	**196.0427**	4.0	(Barbarin)	(0.3)	(6.0)
Kjaerin ($C_9H_9NO_2S$)	**Yes**	**196.0427**	4.0	(Barbarin)	(0.3)	(12)
Flavonoids[e]						
F1 ($C_{39}H_{50}O_{25}$)	Yes	919.2714	3.1	(Rutin)[f]	0.07	1.7
F2 ($C_{39}H_{50}O_{26}$)	Yes	935.2663	2.9	(Rutin)	n.t.	n.t.
F3 ($C_{27}H_{30}O_{15}$)	Yes	595.1657	3.9	(Rutin)	n.t.	n.t.
F4 ($C_{27}H_{30}O_{16}$)	Yes	**611.1607**	3.7	(Rutin)	n.t.	n.t.
Rutin ($C_{27}H_{30}O_{16}$)	Yes	**611.1607**	4.1	536	0.2	4
Rutin ($C_{27}H_{30}O_{16}$)[f]	Yes	**611.1607**	4.1	309[f]	1.4[f]	38[f]

[a] Precise monoisotopic *m/z* values for extracted ion chromatograms were calculated from sum formulae; isomers are indicated in bold. The $[M+H]^+$ ion was the basis of detection in all cases except for the C_9H_7N fragment of brassinin (**P1**), in which case the proton adduct of the fragment was the basis of detection.

[b] Retention time backed up by authentic reference except for the putative sulfoxides (**P7**, **P8**), in which case the t_R is for the suggested candidate peaks.

[c] Slope of the calibration curve in the unit "integration units/nM". Compound names in parentheses indicates that the slope for the indicated compound was used due to lack of an available standard curve for the analyte in question, assuming similar slopes within compound classes.

[d] The lower value is either the limit of detection or the lowest level with detection tested or (in parentheses) an estimated lower limit of detection from dilution series of pure compounds and crude extracts using an assumed slope. The higher range is generally the highest level tested with confirmed linearity, or in case of brassinin (**P1**), nasturlexin A (**P4**) and rutin the confirmed upper limit of linearity. For raphanusamic acid, the additional upper limit (25) denotes the upper range with technically acceptable linearity ($R^2 = 0.98$) but visual signs of detector saturation (Fig. S2I). For brassinin (**P1**), extensive fragmentation to a resonance stabilized indol-3-ylmethylium fragment ion with formula $[M+H]^+ = C_9H_8N^+$ was observed in a concentration-dependent manner. Approximate linearity ($R^2 = 0.93$) in a modest range was observed, while extended approximate linearity ($R^2 = 0.99$) was observed for the C_9H_7N fragment. Screening for minor amounts of **P1** used both extracted ion chromatograms for $[M+H]^+$ and the fragment for improved sensitivity. For nasturlexin A (**P4**), the investigated standard curve to 10 μM was highly curved, likely due to increasing formation of a complex mixture of adducts; approximate linearity suitable for analysis of minor amounts was observed in the indicated range. Abbreviation: n. t.; not tested.

[e] The flavonoid numbers **F1**–**F4** indicate endogenous *Barbarea* flavonoids with known structures, numbers refer to Dalby-Brown et al. (2011); for calculation, standard curves of structurally related rutin were used.

[f] In this range of peak areas, relevant for **F1** in G-type samples, the calibration curve was reasonably well described ($R^2 = 0.9896$) by peak area = 309.0 x + 873,069, where x = [Rutin] in nM. A dilution series of **F1** showed a similar slightly curved shape (Fig. S3G), suggesting that **F1** levels could be safely estimated with the rutin standard curve in the range found in samples although the absolute concentration remained unknown.

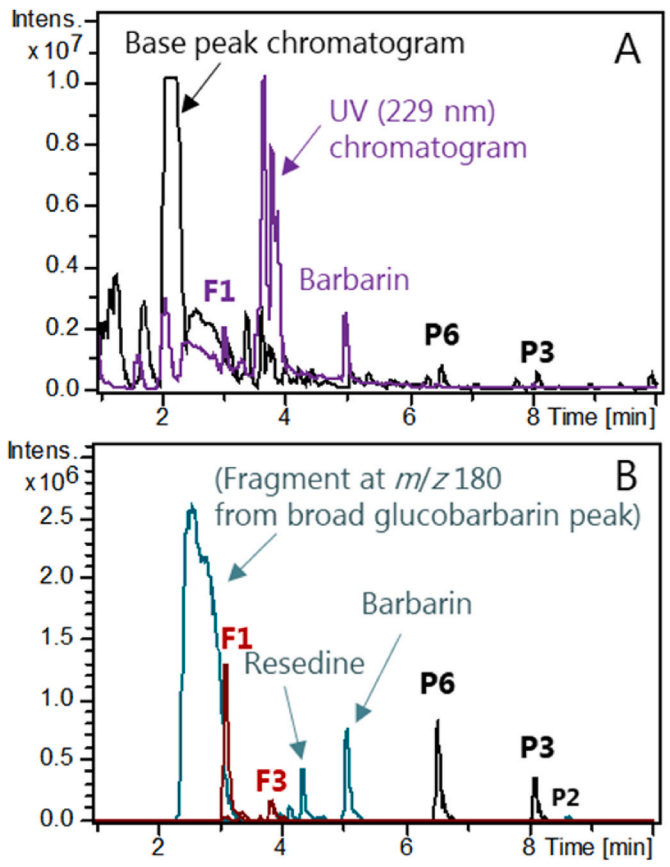


Fig. 4. Representative UHPLC-MS trace of a G-type *Barbarea vulgaris* leaf sample, showing a sample (Day 3, treated) with relatively high levels of phytoalexins (**P3**, **P6**) and glucosinolate hydrolysis products (resedine, barbarin). A. MS base peak chromatogram and UV (229 nm) chromatogram. For selected peaks that were distinguishable in these unspecific traces, identities are indicated. B. Extracted ion chromatograms of selected analytes using the calculated exact *m/z* value for $[M+H]^+$ ions ±0.005 Da for metabolites up to 500 Da and ±0.01 Da for higher masses.

The phytoalexin peaks were generally the only prominent peaks observed at their *m/z* values (±0.005 Da) (Fig. 4); two were isomers (**P2** and **P3**) but were baseline separated (Table 1). Some phytoalexins did not fragment during the QToF MS analysis, while others exhibited characteristic, logical fragments verified by MS2 (Fig. S1). The peak for barbarin had the same elemental composition as a prominent fragment of BAR/EBAR but was otherwise the only major peak at this *m/z* value (Fig. 4, Table 1). The peak for resedine was also the only major peak for this *m/z* value, but in this case, numerous minor peaks at other retention times were also observed. Logical MS2 spectra of barbarin and resedine supported identifications (Figs. S2A–B).

It is well established that the GSL products barbarin and resedine occur as pairs of enantiomers (Fig. 3) reflecting the stereochemistry of their precursors, BAR and EBAR. Whether kjaerin is likewise a pair of enantiomers was uncertain, as the precursor in this case is mainly one stereoisomer (4hEBAR). Using a chiral column, we detected a pair of stereoisomers in 1:1 ratio of natural kjaerin isolated from myrosinase-catalyzed hydrolysis of 4hEBAR (Fig. S2C), suggesting a racemization during the formation of kjaerin as previously suggested from lack of optical activity (Agerbirk and Olsen, 2015). However, at the achiral analysis conditions generally used in this paper, each enantiomeric pair naturally appeared as a single peak. Hence, they are referred to in singularis in the rest of the text: barbarin, resedine, kjaerin. At the general UHPLC conditions of this paper, kjaerin and the isomer *m*-hydroxybarbarin co-eluted (Figs. S2D–E), reflecting a gradient optimized for the less polar phytoalexins. However, MS2 spectra differed (Figs. S2F–G), and we have previously reported conditions for their separation (Agerbirk and Olsen, 2015).

Standard curves showed linearity well above the level of phytoalexins and GSL hydrolysis products detected in leaf samples (Table 1). In contrast, GSLs exhibited broad, overlapping "peaks" early in these chromatograms (ca. 2.2–3.2 min), probably due to their much higher levels and hydrophilicity. Therefore, GSLs were determined after desulfation of GSLs in the remaining half of the crude extract (Section 4.6.). While phytoalexin standard curves were in most cases linear in the ranges tested, saturation was observed for raphanusamic acid (Figs. S2H–I). Raphanusamic acid peak areas from root samples were much higher than the upper linear range of the standard curve, so raphanusamic acid was not quantified from root samples. The phytoalexins **P1** and **P4** (not prominent in the samples analyzed) showed linearity in a restricted range for the $[M+H]^+$ ion, probably due to a high tendency for fragmentation (Fig. S1).

Identified *Barbarea* flavonoids in this text are numbered as in a previous publication (Dalby-Brown et al., 2011), supplemented by "F" for flavonoid, e.g. **F1** for the main flavonoid discussed (Table 1). The four tested flavonoids were previously known from the G-type of *B. vulgaris* only, and the presence of all four were confirmed by extracted ion chromatograms using stringent *m/z* values (±0.01 Da) (Figs. S3A–B). Furthermore, MS2 spectra of flavonoids agreed with known glycoside moieties and supported identification (Fig. S3C). **F1**, **F2** and **F3** were the major peaks of the corresponding *m/z* value in their extracted ion chromatograms, while **F4** was a minor peak (Figs. S3D–E). The tetraglycosylated **F1** and **F2** were absent or near the limit of detection in P-type samples (Fig. S3D). In G-type plants, the major peak in extracted ion chromatograms targeting **F4** was provisionally named 'isoF4a' and eluted 0.2 min earlier than **F4**; several other apparent isomers were observed (Figs. S3B–E). The diglycosylated **F3** or a coeluting isomer was detected in the P-type, while putative **F4** was absent or at low levels in P-type samples (Fig. S3E).

Due to the small amounts of **F1**–**F4** available, concentrations of the flavonoid standards could not be determined gravimetrically. Thus we estimated concentrations using a standard curve of rutin, a commercially available flavonoid (Fig. S3F). Slight detector saturation was observed in standard curves of the flavonoid rutin (Fig. S3F), but the standard curve exhibited an extended approximately linear part (R^2 = 0.99) useful in our range of peak areas (Table 1, Fig. S3F). Peak areas of the main investigated flavonoid **F1** were also higher than the strictly linear portion of the rutin standard curve but were within an approximately linear part. As a standard curve of **F1** itself showed similar shape as the rutin curve (Fig. S3G), the pseudo linear part of the rutin curve was used for **F1** (Table 1).

2.2. The phytoalexin response to $CuCl_2$ of both G-type and P-type *Barbarea vulgaris* was dominated by nasturlexin D and cyclonasturlexin

Leaves of rosette plants of *B. vulgaris* are of the compound type: the petiole-midvein axis carries a number of small lateral lobes as well as a large terminal lobe. Aiming at investigating a homogeneous plant part, we sampled and extracted terminal lobes of rosette leaves for phytoalexin analyses. All leaf samples and analyses in this paper concern rosette leaf terminal lobes, which for simplicity will be termed "leaves" unless specificity is required in the context.

In leaves of *B. vulgaris* plants treated with a spray of 10 mM aq. $CuCl_2$, three phytoalexins were conclusively detected in both genotypes (G and P), the indole phytoalexins cyclobrassinin (**P2**) and cyclonasturlexin (**P3**) and the phenyl-containing phytoalexin nasturlexin D (**P6**). These three are referred to as the three major phytoalexins in the rest of the paper. In all three cases, we detected substantial intensity extracted ion peaks of proton adducts at stringent conditions (±0.005 Da). We also observed the expected *m/z* values, corresponding to $[M+H]^+$ and any fragments exhibited by authentic standards, as major signals in the detected peaks of several samples (Fig. S4A). Cyclobrassinin (**P2**) was

consistently detected at lower levels than **P3** and **P6**. Hence, cyclonasturlexin (**P3**) and nasturlexin D (**P6**) are referred to as the two dominating phytoalexins. In many samples, cyclobrassinin (**P2**) was not even detected despite the presence of the two dominating phytoalexins (Fig. 5).

After preliminary experiments for optimizing extraction, three elicitation experiments were carried out, referred to as experiments 1, 2 and 3, respectively (Section 4.3; Table 2). In all three, the phytoalexins and various other metabolites listed in Table 1 were quantified using a single UHPLC-QToF MS analysis. In experiments 2 and 3, this analysis was supplemented with quantification of GSLs, requiring a separate analytical approach (Section 4.6.). After comparison of leaf positions in experiment 1 (Fig. S5A), we concluded that the youngest fully or nearly fully expanded leaves of a rosette plant were representative and generally high in phytoalexins after $CuCl_2$ treatment; all subsequent leaf analyses considered young rosette leaves. Statistical evaluation was carried out separately for each experiment. The sum of major phytoalexins in treated G-type leaves, averaged across the values at 2 and 3 days after treatment, was on average 7.0 nmol/g fresh wt. (SD 4.6, $N = 6$) in experiment 2 and 8.4 nmol/g fresh wt. (SD 5.4, $N = 10$) in experiment 3. For the P-type (experiment 2), the sum averaged across the values at 1, 2 and 3 days after treatment was 2.6 nmol/g fresh wt. (SD 5.1, $N = 9$).

We manually searched all chromatograms for five other phytoalexins available as standards (**P1**, **P4**, **P5**, **P8**, **P10**) (Table 1), but in no case conclusively detected any of them. However, trace signals were observed in some cases (Fig. S4B). In experiments 1 and 2 we concluded that none of these five phytoalexins were detectable above mere trace levels. This was likewise concluded in experiment 3. However, in experiment 3 we manually integrated all trace peaks for inclusion in statistical tests; very low levels of brassinin (**P1**), nasturlexin C (**P5**) and tridentatol C (**P10**) in the data reflect such trace peaks but not conclusive analytical identification in any sample. Likewise, minute levels of an isomer of **P6** were included in the data for statistical reasons. From reasonable t_R and m/z it was tentatively identified as the known nasturlexin C sulfoxide **P7** (Pedras et al., 2015) (found: m/z 224.0196 ± 0.0023 (mean ± SD, $N = 6$), calculated for $C_{10}H_{10}NOS_2^+$: 224.0198). However, **P7** was not available as authentic standard. Finally, a low intensity peak at 4.7 min tentatively identified as the known nasturlexin D sulfoxide (**P8**) (Pedras et al., 2015) was detected in many samples. The m/z value matched the expected mass of the proton adduct $[M+H]^+$ of the previously reported **P8** (found: m/z 240.0138 ± 0.0019 (mean ± SD, $N = 10$), calculated for $C_{10}H_{10}NO_2S_2^+$: 240.0147). An apparent isomer at 3.6 min was less frequently observed, usually with lower peak area.

The two dominating phytoalexins **P3** and **P6** were generally present in leaves of $CuCl_2$-treated plants 1–3 days after treatment: in both experiment 2 and 3, each sample of a treated (G-type) plant contained both of these two dominant phytoalexins. However, in experiment 1, where only sub-samples of dried leaves were sampled, **P3** was entirely absent from seven of 16 samples of treated plants (44%), while **P6** was consistently detected in all samples of treated plants. We interpreted this observation as evidence of anatomical heterogeneity of distribution of the major indole phytoalexin **P3** in individual leaves, and for this reason, each extracted sample consisted of one entire leaf terminal lobe in the subsequent experiments 2 and 3.

We concluded that the indole phytoalexins cyclobrassinin (**P2**) and cyclonasturlexin (**P3**) (Fig. 1) and the phenyl-containing phytoalexin nasturlexin D (**P6**) (Fig. 2) were the major phytoalexins in leaves elicited by foliar $CuCl_2$ treatment in both the G-type and P-type of *B. vulgaris*, with typical combined average levels between 1 and 10 nmol/g fresh wt.

2.3. Modest phytoalexin time-course differences between G- and P-type *Barbarea vulgaris*

The time course of the phytoalexin response in both plant genotypes was considered in experiment 2. In the control plants, phytoalexins were not detected except a trace in a single G-type plant on day 3 (Fig. 5, Fig. S6). In both plant genotypes, the phytoalexin accumulation of treated plants appeared similar in the first two days. In the G-type (treated compared to controls), there was a significant effect of the treatment on phytoalexin levels (Fig. 6A–C), which did not decline on day 3. In the P-type (treated compared to controls), the period with maximum phytoalexin levels tended to be confined to day 1 or 2, and hence be briefer than in the G-type (Fig. 6A–C). Statistical analysis of the P-type phytoalexin levels (ANOVA) showed a significant effect

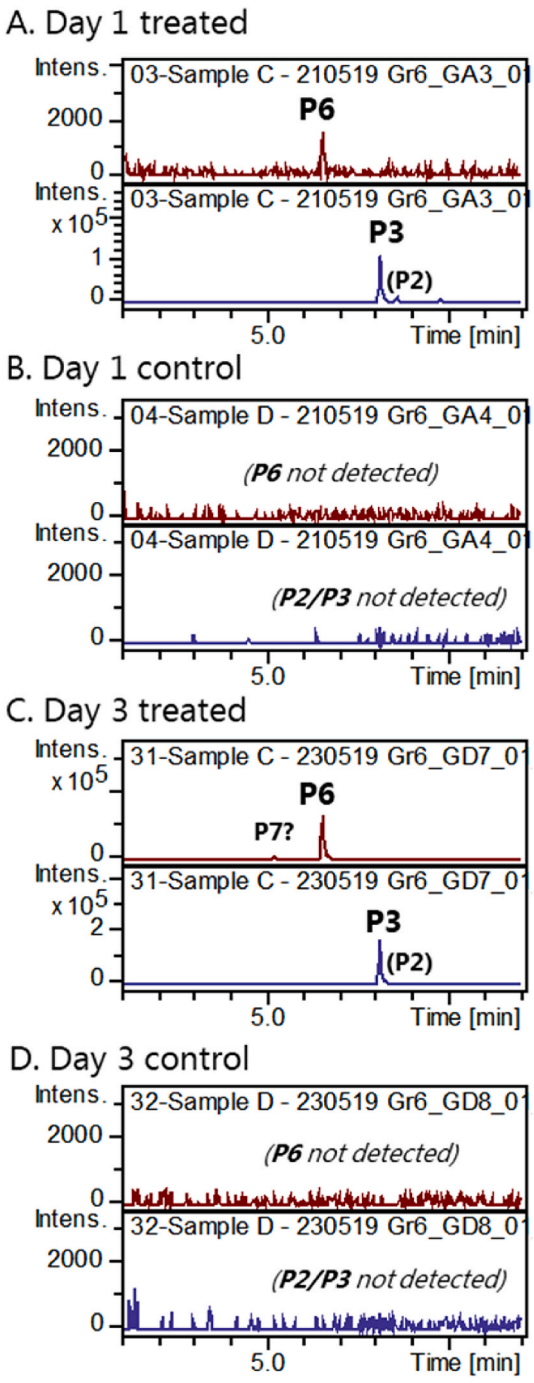


Fig. 5. Representative UHPLC-MS data for treated and control G-type plants in experiment 2. In each panel, the upper trace represents the extracted ion chromatogram (± 0.005 Da) for $[M+H]^+$ of the phenyl containing phytoalexin **P6** and any isomer, while the lower trace represents the extracted ion chromatogram for the indole phytoalexins **P2**, **P3** and any isomer. The legends in panels A–D specify day and treatment/control.

Table 2
Main characteristics of three experiments (Section 4.3.) considering metabolites in leaves after spraying *B. vulgaris* plants with either an aqueous solution of $CuCl_2$ ("treated") or pure water as a mock treatment ("control").

Experiment	Plant types	Days after treatment	Leaf positions[a]	Roots included	GSLs included?	Number of G/P plants	$N_{treated}$: $N_{control}$[b]
Experiment 1	G + P	2	2, 3, 4, 5	No	No	6/4	2:1/3:1
Experiment 2	G + P	1, 2, 3	2	No	Yes	18/18	1:1
Experiment 3	G	1, 2, 3	2	Yes	Yes	30/0	1:1

[a] Counted from the youngest visible leaf in the rosette (not yet fully developed) defined as position 1.
[b] Number of treated plants: number of controls.

(cyclobrassinin, **P2**), a tendency (cyclonasturlexin, **P3**) or no significant effect (nasturlexin D, **P6**) of the treatment.

We then considered whether there was a difference in the phytoalexin response among the plant genotypes. Comparison of the overall phytoalexin response to $CuCl_2$ treatment of the G-type and the P-type by ANOVA showed no statistically significant difference of the responses among the two plant types for any of the three major phytoalexins (Fig. 5, statistical details not shown). Due to the tendency for a briefer response in the P-type (Fig. 6A–C), this genotype was not used in subsequent experiments. However, the data did allow investigation of correlation patterns among individual metabolites.

In individual leaves, levels of the two indole phytoalexins (**P2** and **P3**) appeared to be quite well correlated ($R^2 = 0.66$) in the P-type (Fig. 6D). However, in the G-type, levels of the two indole phytoalexins were not correlated ($R^2 = 0.12$), reflecting the extended duration of the **P3** response. In contrast, levels of the dominant indole phytoalexin **P3** were reasonably well correlated with levels of **P6** in the G-type ($R^2 = 0.78$), while any correlation in the P-type relied on a single pair of observations (Fig. 6E). This pattern of variable degrees of correlation between phytoalexin levels supported the tendency for two contrasting time courses of accumulation: some phytoalexins tended to peak early (day 1–2, all phytoalexins in P-type, cyclobrassinin in G-type), while the two dominant phytoalexins tended to peak later in the G-type (day 2–3) (Fig. 6A–C). The lack of correlation of early **P2** with later **P3** and **P6** in the G-type was confirmed by statistical testing in experiment 3 (vide infra). In both plant genotypes, low levels of putative nasturlexin D sulfoxide (**P8**) were identified in many samples. Levels of the putative sulfoxide **P8** appeared to be well correlated with **P6** levels as expected for a proposed downstream metabolite of **P6** ($R^2 = 0.81$ in both types) (Fig. 6F).

From the comparison of the two plant genotypes in experiment 2, we concluded that the same three major phytoalexins were formed in both plant types, with no statistically significant difference in the response. As the combined data suggested that the response to $CuCl_2$ treatment was more prolonged in the G-type than in the P-type, we concentrated on the G-type in experiment 3.

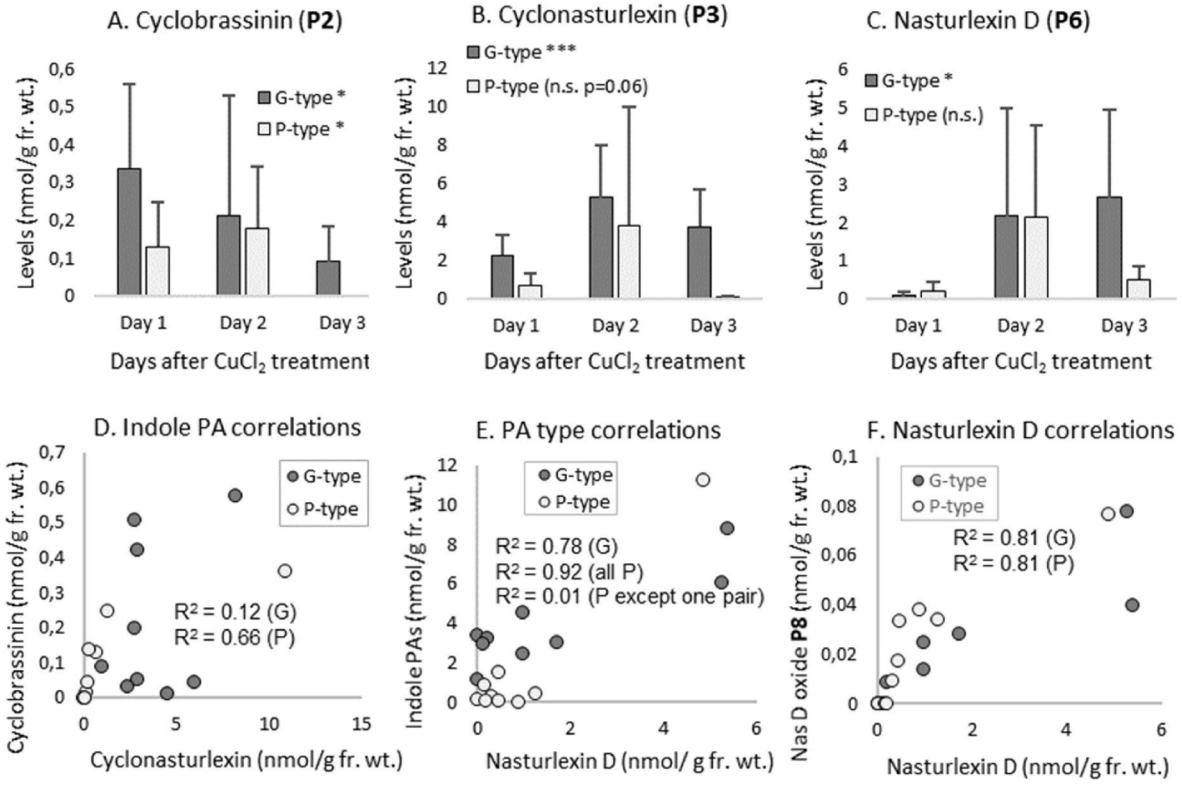


Fig. 6. Phytoalexin response in young rosette leaves to $CuCl_2$-treatment of leaves in two genotypes (G-type and P-type) of the plant *Barbarea vulgaris*. $N = 3$ treated and 3 control plants of each plant type on each day; since control plants were generally devoid of phytoalexins except a trace of nasturlexin in one control G-type on day 3, only levels for treated plants are shown. A-C, levels of individual phytoalexins as a function of time after elicitation; D-F, pairwise correlation plots of phytoalexins or structural groups of phytoalexins, each dot refers to the same leaf. Data in plots A-C were analyzed by two-way ANOVA; statistical significance of effect of treatment (H_0: no effect of treatment) is indicated as follows: *, $P < 0.05$; **, $P < 0.01$; ***, $P < 0.001$; n. s., not significant. No significant effects of day or treatment x day effect was found for any of the three phytoalexins. Bars indicate means, whiskers indicate standard deviations. In E, the correlation analysis of the P-type dataset was repeated after omission of one observation pair, showing that the apparently high correlation was due to this observation pair only and hence with low support.

In experiment 3, with focus on the G-type, higher number of replicates and consideration of both leaves and roots, the effect of the $CuCl_2$ treatment was confirmed for all three major phytoalexins in leaves (Table 3). However, to our surprise, low levels of phytoalexins were detected also in control plants (Fig. S7), suggesting that phytoalexin biosynthesis in all plants was already elicited (by an uncontrolled environmental factor e.g. pathogen exposure) to a low extent at the time of the $CuCl_2$ or mock treatments. No visible signs of pathogen attack or other stress were noticed during the experiment. The phytoalexin profile from this background-elicitation was dominated by the phenyl-containing phytoalexin **P6**; levels tended to decline over the three experimental days (Table 3).

Traces of the suggested precursor of **P6**, nasturlexin C (**P5**) and its sulfoxide **P7** were also detected in the leaves, but not the suggested earlier precursor nasturlexin A (**P4**) (Table 3). Very low levels of the parent indole phytoalexin brassinin (**P1**) and the phenyl-containing phytoalexin tridentatol C (**P10**) were also tentatively detected. Analysis of variance (ANOVA) suggested that levels of these trace phytoalexins depended on the treatment, with highest levels in treated plants (Table 3). There was no statistically significant effect of treatment for the putative nasturlexin D sulfoxide (**P8**); however, linear regression analysis of levels of **P8** as a function of nasturlexin D (**P6**) showed a statistically highly significant positive slope, both when considering treated plants or control plants (Table 4). This result was expected for an obvious precursor-product relation and agreed with correlations observed in experiment 2 (Fig. 6F).

In order to test the tentative observations from experiment 2 of different time courses of appearance of the modest level indole phytoalexin **P2** versus the dominant indole phytoalexin **P3** and phenyl-containing **P6**, correlation analysis was supplemented by linear regression analysis using data for experiment 3 (Table 4). Levels of the indole phytoalexin **P2** were not correlated with any of the two dominant phytoalexins, reflecting the different timing of their elicitation, with **P2** peaking early (day 1) and the two major phytoalexins **P3** and **P6** continuously accumulating over three days (Fig. S7). This result agreed with tendencies and correlation analysis for the G-type in experiment 2. In contrast, levels of the two major phytoalexins **P3** and **P6** were correlated (Table 4), as also inferred for the G-type in experiment 2 and in agreement with similar appearance of averaged time course plots (Fig. S7).

Due to known high levels of the expected precursor GSLs PE and IM in roots, we had anticipated that phytoalexin biosynthesis might take place in roots as a systemic response to $CuCl_2$ treatment of leaves (Koprivova et al., 2023). However, only trace values of nasturlexin D (**P6**) were detected in roots, with no statistical association to $CuCl_2$ treatment. Among the phytoalexins searched for (Table 1), no other phytoalexin was detected in roots of G-type plants (Table 3).

2.4. Variable dynamics of indole glucosinolates after phytoalexin elicitation

The dominating indole GSL in all leaf samples was IM. Although IM is the expected biosynthetic precursor of indole phytoalexins (Fig. 1), biosynthesis of indole phytoalexins did not require any significant drain of IM levels, as IM levels were typically 1–2 orders of magnitude higher than levels of indole phytoalexins. However, in experiment 2 a moderate decline of IM levels in treated plants was observed in G-type plants, while IM levels were not affected in P-type plants. In experiment 3, levels of IM in G-type plants were likewise not affected by the treatment (Table 5, Fig. 7A). Accordingly, we concluded that IM levels were not

Table 3
Levels (nmol/g fresh wt.) of phytoalexins in young rosette leaves or roots after $CuCl_2$-treatment ("treated") or mock treatment ("control") of G-type *Barbarea vulgaris* plants ($N = 5$ in each of six groups; data from experiment 3). Bold font names and data indicate the three major phytoalexins and their levels.

Phytoalexin		Levels in control plants			Levels in treated plants			Stat. sign. ANOVA		
		Day 1	Day 2	Day 3	Day 1	Day 2	Day 3	Tr.	Day	Tr. x Day
Rosette leaves[a]										
Brassinin (**P1**)[b]	m	n.d.	0.0005	n.d.	0.015	0.006	0.009	**	n.s.	n.s.
	sd	–	0.001	–	0.016	0.009	0.012			
Cyclobrassinin (P2)	m	**n.d.**	**n.d.**	**0.002**	**0.20**	**0.11**	**0.004**	***	*	*
	sd	–	–	5 E−6	0.11	0.13	0.01			
Cyclonasturlexin (P3)	m	**0.35**	**0.26**	**0.28**	**0.94**	**3.0**	**4.7**	***	*	**
	sd	0.53	0.42	0.45	0.43	1.8	2.4			
Nasturlexin C (**P5**)[b]	m	n.d.	0.0004	0.0017	0.015	0.0079	0.013	**	n.s.	n.s.
	sd	–	0.0009	0.0037	0.012	0.0094	0.015			
Nasturlexin D (P6)	m	**1.7**	**1.0**	**0.93**	**0.93**	**3.3**	**5.8**	*	n.s.	n.s.
	sd	1.9	1.4	1.5	0.91	2.5	5.0			
Nasturlexin C ox (**P7**)[b]	m	0.013	0.004	0.011	0.007	0.042	0.064	***	n.s.	*
	sd	0.014	0.006	0.018	0.006	0.032	0.044			
Nasturlexin D ox (**P8**)[b]	m	0.032	0.011	0.025	0.021	0.064	0.069	n.s.	n.s.	n.s.
	sd	0.050	0.013	0.029	0.038	0.053	0.046			
Tridentatol C (**P10**)[b]	m	0.0011	n.d.	0.0027	0.0087	0.0048	0.044	***	*	*
	sd	0.0025	–	0.0059	0.0078	0.0048	0.040			
Roots[c]										
Nasturlexin D (**P6**)	m	0.005	0.013	0.017	0.010	0.006	0.007	n.s.	n.s.	n.s.
	sd	0.007	0.009	0.014	0.004	0.003	0.005			

The names 'nasturlexin C ox' and 'nasturlexin D ox' refer to the known sulfoxides (**P7**, **P8**) not backed up by authentic standards. Abbreviations: Tr., treatment, Tr. x Day, statistical interaction between treatment and day; m, mean; sd, standard deviation. Statistical significance in analysis of variance (Stat. sign. ANOVA, H_0: no difference between controls and treated plants) is indicated as follows: *, $P < 0.05$; **, $P < 0.01$; ***, $P < 0.001$; n.s., not significant.

[a] Additional data for leaves: Nasturlexin A (**P4**) was not detected in any leaf sample. A trace of nasturlexin B (**8**) (0.001 nmol/g fresh wt.) was detected in one leaf sample. The reported trace levels of brassinin (**1**) were based on manual integration of trace peaks of the *m/z* 130 fragment ion, a peak for the $[M+H]^+$.ion was not detected in any sample.

[b] Inconclusive identification of **P5**, **P7**, **P8** and **P10** due to very low levels close to detection limit. These five metabolites were detected as trace-like peaks tentatively identified by retention time of stringent (±0.005 Da) extracted ion chromatograms only; due to low levels, correct fragmentation could not be confirmed. Levels of these five metabolites should hence be regarded as tentative maximum estimates only.

[c] Additional data for roots: Nasturlexin A (**P4**) traces (typically 0.002 nmol/g fresh wt.) were detected in six root samples with no correlation to treatment. Traces of nasturlexin C (**P5**) were detected in one control (0.005 nmol/g fresh wt.) and one treated (0.010 nmol/g fresh wt.) root sample. Trace *m/z* 130 peaks at the t_R of brassinin (**P1**) were detected in some root samples, with no difference between controls and treated plants. No other tested phytoalexins were detected in any roots sample.

Table 4
Correlation and linear regression analysis of levels of selected phytoalexins in young rosette leaves of *Barbarea vulgaris* the G-type plants, using either $CuCl_2$ treated plants (T) or mock-treated control plants (C). Mock-treated plants contained low levels of nasturlexin D (**P6**) apparently due to background elicitation not caused by the experimental treatment. Data from experiment 3.

x-Variable	y-Variable	T/C	R^2	Linear regression statistics					*N*
				Intercept	Stat. sign.	Slope	SE	Stat. sign.	
Nasturlexin D (**P6**)	Nasturlexin D ox (**P8**)	T	0.75	0.014	n.s.	0.011	0.002	***	15
Nasturlexin D (**P6**)	Nasturlexin D ox (**P8**)	C	0.61	0.003	n.s.	0.016	0.004	***	15
Cyclonasturlexin (**P3**)	Cyclobrassinin (**P2**)	T	0.09	0.15	*	−0.016	0.014	n.s.	15
Nasturlexin D (**P6**)	Cyclonasturlexin (**P3**)	T	0.37	1.6	*	0.38	0.14	*	15
Nasturlexin D (**P6**)	Cyclobrassinin (**P2**)	T	0.06	0.13	**	−0.008	0.009	n.s.	15

Nasturlexin D ox (**P8**) refers to a putative nasturlexin sulfoxide (Fig. 2) not backed up by an authentic standard. Abbreviations: T, treated plants; C, control plants, R^2, squared correlation coefficient; Stat. sign, statistical significance; SE, standard error; *N*, number of data pairs. Statistical significance in linear regression analysis (H_o: the relevant parameter = zero) is indicated as follows: *, $P < 0.05$; **, $P < 0.01$; ***, $P < 0.001$; n.s., not significant.

generally affected by the $CuCl_2$ treatment.

Searching for any yet poorly understood metabolic connection (Pedras et al., 2008) between phytoalexins (such as the 4-substituted **P3**) and 4-substituted indole GSLs, we compared levels of 4-substituted indole GSLs in treated and control plants. The 4-substituted indole GSLs were 4-hydroxyindol-3-ylmethylGSL (4hIM) and 4-methoxyindol-3-ylmethylGSL (4moIM) (Fig. 1). In experiment 2, comparing both plant genotypes, highly significant effects of considerable magnitude were observed for levels of 4-substituted indole GSLs, but in opposite directions and with different levels in control plants (Table 5, Fig. S8A, Fig. S9). In experiment 3, however, treated and control G-type plants showed comparable levels of 4-substituted indole GSLs (Table 5, Fig. 7B). We concluded that the $CuCl_2$ treatment resulted in a strong apparent effect on levels of 4-substituted indole GSLs in some but not all experiments, but the timing and direction of the fluctuation was not reproducible.

2.5. Depletion of phenethylglucosinolate during phytoalexin elicitation

Two phenyl-containing GSLs had been suggested as precursors in the biosynthesis of the phenyl-containing phytoalexin **P6**: either the unsubstituted PE and/or the *meta*-hydroxy derivative 3 hP E. However, the latter was not detectable in these *B. vulgaris* accessions (Fig. S10), while PE was consistently detected (Fig. S11).

In the P-type, PE levels were significantly affected by number of days after elicitation, reflecting quite low levels of PE in treated plants on days 1 and 2 compared to controls (Table 6, Fig. S12). The treatment effect was trending, but not statistically significant (P = 0.11), perhaps reflecting that levels had returned to control levels on day 3, at which day **P6** accumulation had also ceased. Since our aim was to test whether on-going biosynthesis of **P6** resulted in decreased levels of PE due to PE being a precursor of **P6**, testing PE levels within the entire 3-day duration of the data was misleading. Indeed, exclusion of day 3 data resulted in a highly significant treatment effect in ANOVA (Table 6). In the G-type, significantly lowered levels of PE were observed in both experiment 2 and 3 (Table 6, Fig. 7C, Fig. S12). We concluded that PE levels were reproducibly reduced in treated plants during phytoalexin accumulation.

If phytoalexin biosynthesis involved unspecific GSL hydrolysis (Fig. 3), a general lowering of levels of all GSLs or all phenyl-containing GSLs could be hypothesized. Phenyl containing GSLs dominated the GSL profile of leaves, with total mean levels typically three orders of magnitude higher than levels of phenyl containing phytoalexins (compare Tables 3 and 6). For the P-type, there was no significant difference in total GSLs or total phenyl-containing GSLs in treated versus control plants when considering all three experimental days. However, for this genotype, phytoalexin accumulation was restricted to the first two experimental days, and there was a modest treatment effect when considering the first two days only (Table 6). For the G-type, lowered total GSLs and total phenyl-containing GSLs were found in treated plants compared to controls in experiment 2, but in experiment 3 the trend was different, with increased levels on day 2 and decreased levels on day 3 (Table 6, Fig. 7D). We concluded a tendency for lowered or fluctuating total GSL levels accompanying $CuCl_2$ treatment. We further investigated the hypothesis based on GSL product levels (Section 2.6.).

Other hydroxyphenyl-containing GSLs were searched for as potential indications of hydroxylation of PE or derivatives in the *meta* position. The data agreed with previous investigations (Agerbirk et al., 2015), showing low levels of 4hEBAR and 3hEBAR in the P-type and absence or very low levels in the G-type (Fig. S12). No relation to $CuCl_2$ treatment

Table 5
Levels of indole glucosinolates (GSLs) in young rosette leaves after $CuCl_2$-treatment ("treated") or mock treatment ("control") of G-type and P-type *Barbarea vulgaris* plants on the day before Day 1.

GSL		Levels in control plants			Levels in treated plants			Stat. sign. ANOVA		
		Day 1	Day 2	Day 3	Day 1	Day 2	Day 3	Tr.	Day	Tr.xDay
Indol-3-ylmethylGSL (IM) (μmol/g fresh wt.)										
Exp. 2, P-type	m	0.28	0.27	0.39	0.13	0.28	0.65	n.s.	n.s.	n.s.
	sd	0.11	0.15	0.27	0.07	0.006	0.58			
Exp. 2, G-type	m	0.23	0.65	0.83	0.09	0.28	0.40	**	**	n.s.
	sd	0.12	0.11	0.22	0.06	0.22	0.17			
Exp. 3, G-type	(See Fig. 7A)							n.s.	***	n.s.
Total 4-substituted indole GSLs (4hIM+4moIM)[a] (nmol/g fresh wt.)										
Exp. 2, P-type	m	0.46	4.7	1.0	5.7	15	65	**	**	**
	sd	0.14	5.9	0.8	4.2	1.9	32			
Exp. 2, G-type	m	8.2	19	21	1.6	4.2	6.7	***	*	n.s.
	sd	5.0	8.7	10	1.3	2.5	4.3			
Exp. 3, G-type	(See Fig. 7B)							n.s.	**	n.s.

Exp., Experiment; m, mean, sd, standard deviation. Statistical significance in analysis of variance (Stat. sign. ANOVA, H_0: no difference between controls and treated plants) is indicated as follows: *, $P < 0.05$; **, $P < 0.01$; ***, $P < 0.001$; n.s., not significant. Plots of the experiment 2 data are illustrated in Fig. S9.

[a] Levels of 4-substituted indole GSLs essentially reflected levels of 4moIM; the intermediate 4hIM was only detected in few samples and at moderate levels.

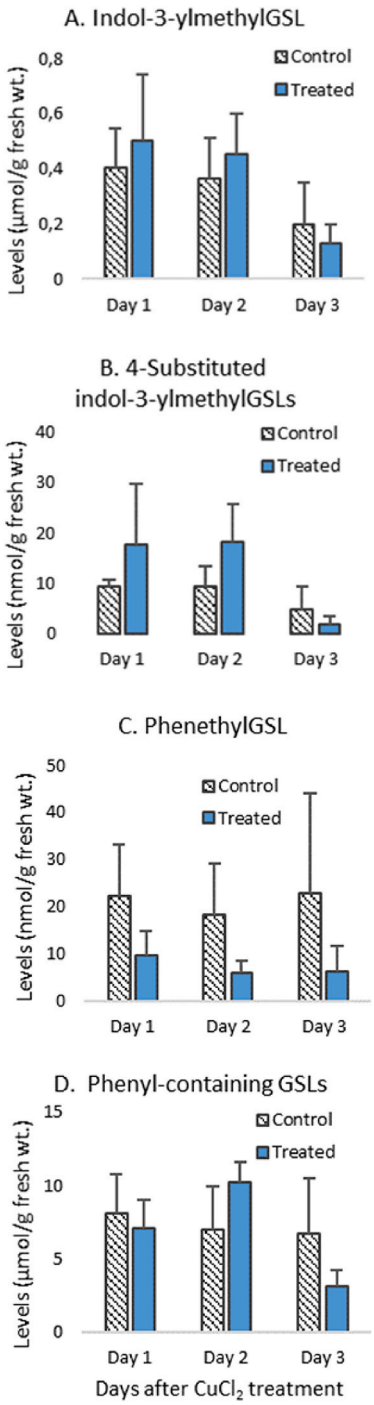


Fig. 7. Levels of selected glucosinolates (GSLs) as a function of time in young rosette leaves of G-type *Barbarea vulgaris* plants after $CuCl_2$-treatment (treated) or mock treatment (control). The GSLs considered are (A) indol-3-ylmethylGSL (IM), (B) the sum of 4-hydroxyIM and 4-methoxyIM, (C) phenethylGSL (PE) and (D) the sum of phenyl-containing GSLs. Bars depict means, whiskers indicate standard deviations. For statistical evaluation, see Table 5 (A, B) and Table 6 (C, D).

was found. During inspections of desulfo GSL chromatograms for trace peaks, an unidentified isomer of (desulfo) 3hPE, BAR and EBAR was consistently detected in chromatograms (Fig. S10). From comparison of retention times, this isomer was distinct from all six known isomeric (desulfo) GSLs (BAR, EBAR, 3hPE, 4hPE and two methoxybenzylGSL isomers) that were all available as authentic desulfo GSL standards (Agerbirk et al., 2022). If this isomer represents a yet unknown GSL, it could potentially be "*ortho*-hydroxy PE" or several other isomers. We considered whether it could possibly be related to an alternative pathway to **P6** (Fig. 2). The unknown isomer was tentatively named "isoBAR" and showed no relation to the $CuCl_2$-treatment (Fig. S13). We concluded that the hypothetic **P6**-precursor 3hPE was not detected and that no detected hydroxyphenyl-containing GSLs showed any relation to $CuCl_2$-treatment.

2.6. Levels of glucobarbarin hydrolysis products depended on $CuCl_2$-treatment and were correlated with phytoalexin levels

For an independent assessment of GSL hydrolysis, levels of GSL products were investigated using linear models. We initially used data from experiment 3 due to the higher number of replicates in that experiment, and subsequently compared with data from experiment 2. Representative chromatograms are illustrated (Figs. S8B–D).

A precursor-product relationship of barbarin and resedine in intact leaves had previously been suggested (Fig. 3), and this suggestion was supported by linear regression analysis of resedine levels as a function of barbarin levels in $CuCl_2$-treated leaves (Fig. 8A). The slope was statistically different from zero ($P < 0.001$), suggesting that levels of resedine indeed were related to levels of barbarin. In control plants and roots, however, no relationship was distinguishable (Fig. 8A, Fig. S14). Data from experiments 1 and 2 agreed with a linear relationship of barbarin and resedine levels in treated leaves (Figs. S15A–B, Figs. S16A–B).

The same approach was used for testing for a statistical relationship of barbarin levels and total levels of glucobarbarins (BAR and EBAR, the known GSL precursors of barbarin). If levels of barbarin in intact plants reflected a steady turnover of glucobarbarins, we expected barbarin levels to be correlated with glucobarbarin levels. However, this was not the case, neither in leaves (Fig. 8B) nor in roots (Fig. S14 B). In experiment 2, similar complex patterns were seen, although a statistically significant ($P < 0.05$) relationship was seen for treated G-type plants (Figs. S15C–D). Experiment 1 could not be included because GSLs were not determined.

Our alternative hypothesis was that barbarin levels were linearly related to phytoalexin levels. That relationship would be expected if phytoalexin biosynthesis is accompanied not only by hydrolysis of precursor GSLs but also hydrolysis of other GSLs. Data from experiment 3 agreed with this hypothesis, as the slope of the regression line of barbarin levels as a function of phytoalexin levels was greater than zero (Fig. 8C). As the glucobarbarins are the dominating GSLs but are considered unlikely phytoalexin precursors (Pedras and To, 2018), this result suggested general GSL hydrolysis (i.e., without structural specificity) accompanying phytoalexin biosynthesis. The linear relationship of barbarin versus total phytoalexins was less robust when tested in experiments 1 and 2; the slope was significantly ($P < 0.01$) higher than zero in one experiment, while the other three only supported the hypothesis by trend (*P*-values 0.13, 0.07, and 0.06, respectively) and showed similar slopes (Fig. S16B; Figs. S17A–B). We concluded that the combined data agreed with barbarin levels generally related to phytoalexin levels.

If indeed barbarin levels were related to total phytoalexin levels because general GSL hydrolysis accompanied GSL hydrolysis for phytoalexin biosynthesis, levels of resedine should similarly be related to total phytoalexin levels. Indeed, there was a statistically highly significant linear relationship ($P < 0.001$) between levels of resedine and combined phytoalexins (Fig. 8D). The relationship of resedine versus total phytoalexins was relatively robust when tested in experiments 1 and 2; slopes were in the same range and in three of four plots a positive slope was statistically significant (Fig. S16C, Figs. S17C–E).

Considering the apparent statistical relation of barbarin and resedine to phytoalexin accumulation, we considered mean levels of these metabolites in the three days following the phytoalexin elicitation (Fig. 9A+B). Barbarin showed a modest ($P < 0.05$) dependency of the $CuCl_2$-treatment (Fig. 9A), while resedine showed a statistically highly

Table 6
Levels of phenethylglucosinolate (PE) as well as the sum of all phenyl-containing glucosinolates (GSLs) and all GSLs in young rosette leaves after $CuCl_2$-treatment ("treated") or mock treatment ("control") of G-type and P-type *Barbarea vulgaris* plants on the day before Day 1. Units for the GSL levels are indicated separately for each entry.

GSL		Levels in control plants			Levels in treated plants			Stat. sign. ANOVA		
		Day 1	Day 2	Day 3	Day 1	Day 2	Day 3	Tr.	Day	Tr.xDay
PhenethylGSL (PE) (nmol/g fresh wt.)										
Exp. 2, P-type	m	37	15	44	1.8	5.0	54	n.s.	**	n.s.
	sd	12	4.0	5.9	0.7	1.4	33			
Same data, excluding day 3 with declined nasturlexin D levels (Fig. 6C):								***	*	**
Exp. 2, G-type	m	4.2	23	21	0.43	5.8	8.2	***	**	n.s.
	sd	4.6	8.1	3.6	0.45	5.3	5.2			
Exp. 3, G-type	(See Fig. 7C)							**	n.s.	n.s.
Total phenyl-containing GSLs (µmol/g fresh wt.)										
Exp. 2, P-type	m	6.6	6.5	8.4	3.1	4.7	6.7	n.s.	n.s.	n.s.
	sd	2.1	2.0	4.7	1.9	1.6	3.4			
Same data, excluding day 3 with declined nasturlexin D levels (Fig. 6C):								*	n.s.	n.s.
Exp. 2, G-type	m	4.8	8.5	9.6	2.5	3.4	2.2	***	n.s.	n.s.
	sd	2.4	2.8	0.14	3.1	1.9	1.4			
Exp. 3, G-type	(See Fig. 7D)							n.s.	**	*
Total GSLs (µmol/g fresh wt.)										
Exp. 2, P-type	m	6.9	6.7	8.8	3.3	4.9	7.4	n.s.	n.s.	n.s.
	sd	2.2	1.9	5.0	2.0	1.6	4.0			
Exp. 2, G-type	m	5.0	9.1	10.4	2.6	3.7	2.6	***	n.s.	n.s.
	sd	2.5	2.9	0.3	3.2	2.1	1.6			
Exp. 3, G-type	m	8.5	7.4	6.9	7.6	10.7	3.3	n.s.	**	*
	sd	2.7	3.1	3.9	2.1	1.5	1.1			

Exp., Experiment; m, mean, sd, standard deviation. Statistical significance in analysis of variance (Stat. sign. ANOVA, H_0: no difference between controls and treated plants) is indicated as follows: *, $P < 0.05$; **, $P < 0.01$; ***, $P < 0.001$; n.s., not significant. Plots of the experiment 2 data are illustrated in Fig. S12.

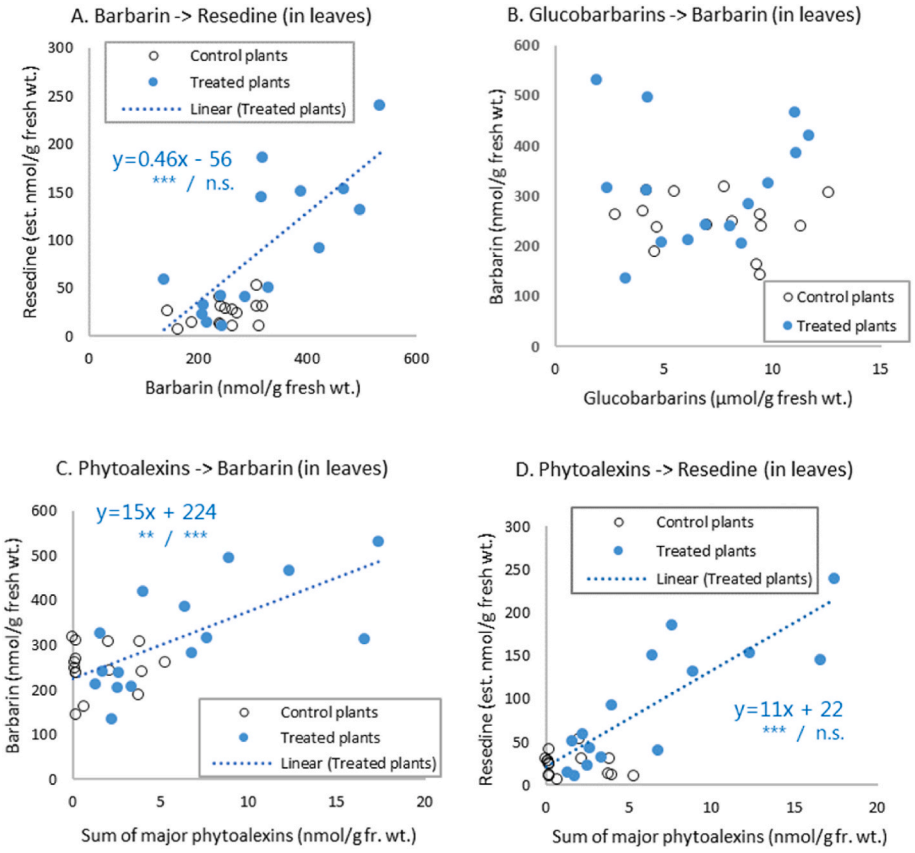


Fig. 8. Plots of levels of selected metabolites in G-type *Barbarea vulgaris* young rosette leaves, after treating plants with $CuCl_2$ (*aq*) or a mock treatment, for testing specific hypotheses of statistical relationships. The logical arrows (->) in legends represent the statistical hypotheses tested, not necessarily a biochemical precursor-product relationship. Linear regression lines with equations for best fit are inserted, statistical significance of slopes and intercepts are shown below the equations; statistical significance (H_0: the relevant parameter = zero) is indicated as follows: *, $P < 0.05$; **, $P < 0.01$; ***, $P < 0.001$; n.s., not significant. A, resedine levels as a function of barbarin levels; 95% confidence interval of the slope was [0.23; 0.69]; B, glucobarbarin levels as a function of glucobarbarin levels, from the observed pattern, linear regression analysis was considered not relevant; C, barbarin levels as a function of the sum of the major three phytoalexins cyclobrassinin (**P2**), cyclonasturlexin (**P3**) and nasturlexin D (**P6**); 95% confidence interval for the slope [5.4; 24.8], for the cut-off [145; 304]; D. Resedine levels as a function of summed **P2**+**P3**+**P6** levels, 95% confidence interval for the slope [6.8; 15.5], for the cut-off [-14; 57].

significant ($P < 0.001$) relationship with much elevated mean levels in treated plants on days 2 and 3 (Fig. 9B).

The accumulation of barbarin and resedine in parallel to phytoalexin elicitation provided a means of estimating the unspecific hydrolysis of glucobarbarins accompanying phytoalexin biosynthesis. The slope with confidence intervals of the regression line of barbarin levels as a function of major phytoalexin levels would suggest hydrolysis of between five and 25 times as much glucobarbarins as the molar amount of precursor GSL channeled into phytoalexin biosynthesis (Fig. 8C). This was a minimum estimate as any barbarin further transformed to resedine was

not included. Linear regression analysis of the sum levels of barbarin and estimated resedine as a function of the sum levels of major phytoalexins suggested a somewhat higher turnover of 14–39 times as much glucobarbarins as precursor GSLs channeled into phytoalexin biosynthesis (Fig. S18). However, this estimate is less certain because resedine levels were estimated using a standard curve for barbarin (Table 1).

Overall, we concluded that phytoalexin accumulation was accompanied by marked accumulation of the downstream GSL metabolite resedine and frequently the GSL hydrolysis product barbarin, indicating appreciable general turnover of GSLs accompanying elicitation of phytoalexins.

In addition to the barbarin-resedine pair from hydrolysis of glucobarbarins, we considered a more general type of GSL metabolite, raphanusamic acid. Raphanusamic acid can be formed from *in vivo* detoxification and turnover of any isothiocyanate; which in *B. vulgaris* could include detoxification of phenethyl isothiocyanate (Fig. 3) and perhaps indol-3-ylmethyl isothiocyanates. The observed levels were of the same order of magnitude as the drop of PE levels during phytoalexin accumulation, and showed statistically significant effects of treatment and time after elicitation, peaking already at day 1 (Fig. 9C). Due to the peak at day 1, a linear relationsship between raphanusamic acid and phytoalexins was not expected. Actually, plots of raphanusamic acid levels as a function of phytoalexin levels had a peculiar hyperbolic character with raphanusamic acid-phytoalexin pairs strongly associated with the x- and y-axes (Fig. S19). That is, high raphanusamic acid levels coincided with less than maximum phytoalexin levels. The plot reflected the early rise and immediate decline of this general isothiocyanate detoxification product after phytoalexin elicitation, in contrast to the steady accumulation of phytoalexins, barbarin and resedine.

Enzymes responsible for the *m*-hydroxylation in **P6** or *p*-hydroxylation in **P9** and **P10** could hypothetically form kjaerin or *m*-hydroxybarbarin. For this reason, we investigated all samples for kjaerin and *m*-hydroxybarbarin. Occasional traces were detected, but neither were conclusively detected in any sample. However, since the limits of detection were rather high relative to phytoalexin levels, relevant levels might be below the limit of detection. We concluded that major levels of kjaerin and *m*-hydroxybarbarin were absent.

Finally, in an attempt to reveal any general metabolic disturbance after $CuCl_2$ elicitation of phytoalexins, we considered flavonoid levels (Pedras et al., 2008). Numerous flavonoid-like peaks were detected in G-type and P-type plants, in agreement with previous reports (Figs. S3D–E). We selected the dominant of the four identified flavonoids, tetraglycosylated flavonoid **F1**, as a representative of general accumulated metabolites in G-type *B. vulgaris*. Analysis of variance revealed no statistically significant differences between **F1** levels in treated versus control plants (Fig. S20).

3. Discussion

In this study of two genetically well-characterized genotypes of the crucifer *Barbarea vulgaris*, G-type and P-type, we have characterized phytoalexin responses to foliar $CuCl_2$ treatment (a known elicitor of phytoalexins): mainly the indole phytoalexin **P3** (cyclonasturlexin) and the phenyl-containing phytoalexin **P6** (nasturlexin D), and lesser amounts of the indole phytoalexin **P2** (cyclobrassinin). Two suggested precursor GSLs, the phenyl-containing PE and the indole-containing IM, were present in leaves. A third suggested precursor, 3hPE, a derivative of PE which is extremely rare in nature, was not present above the limit of detection. We have additionally performed a first characterization of the additional metabolic response to $CuCl_2$ treatment, with focus on interactions with GSL hydrolysis. Four interactions with GSL hydrolysis were particularly evident. First, depletion of PE during the first three days after elicitation, as expected if the phenyl-containing GSL PE is precursor of the biosynthesis of phenyl containing **P6**. Second, a brief accumulation of raphanusamic acid, a known product of the turnover of isothiocyanates (Pastorczyk and Bednarek, 2016; Jeschke et al., 2019; Sugiyama et al., 2021), on the first day after elicitation. Third, continued accumulation of products of the turnover of a pair of non-precursor GSLs, the glucobarbarins BAR and EBAR, during the first three days after elicitation. Levels of these products of GSL turnover, barbarin and resedine, also correlated with phytoalexin levels. The statistical association with phytoalexin levels and $CuCl_2$ treatment was particularly strong for the down-stream product resedine. Fourth, drastic fluctuations of 4-substituted indole GSLs were observed to accompany the treatment but in a poorly reproducible way. In contrast, no *m*-hydroxyphenyl-containing GSLs or GSL products showed increased levels associated with phytoalexin biosynthesis, suggesting that anticipated *m*-hydroxylation in phytoalexin biosynthesis did not happen to GSLs or their products.

Combining phytoalexin biosynthesis from IM and PE appears to be unusual among crucifers, which usually produce phytoalexins from the parent indole GSL IM (Pedras et al., 2011). From patterns of correlation or lack of it, we tentatively observed that the biosynthesis of the two indole phytoalexins **P2** and **P3** differed in timing in the G-type, while their timing was more consistent in the P-type. Similarly, we observed a signature of different timing of the phenyl-containing phytoalexin **P6** between the two genotypes. Overall, these observations suggest a somewhat different biosynthesis and regulation of each of the three major phytoalexins in our genotypes, although the kinds of phytoalexins were identical. Different time courses, brief or extended, could have biological consequences in interactions with pathogens. In general, the results of decades of study of interactions between GSLs, phytoalexins and detrimental as well as beneficial microbes are accumulating (Plaszkó et al., 2022; Poveda et al., 2020). In contrast, identification of

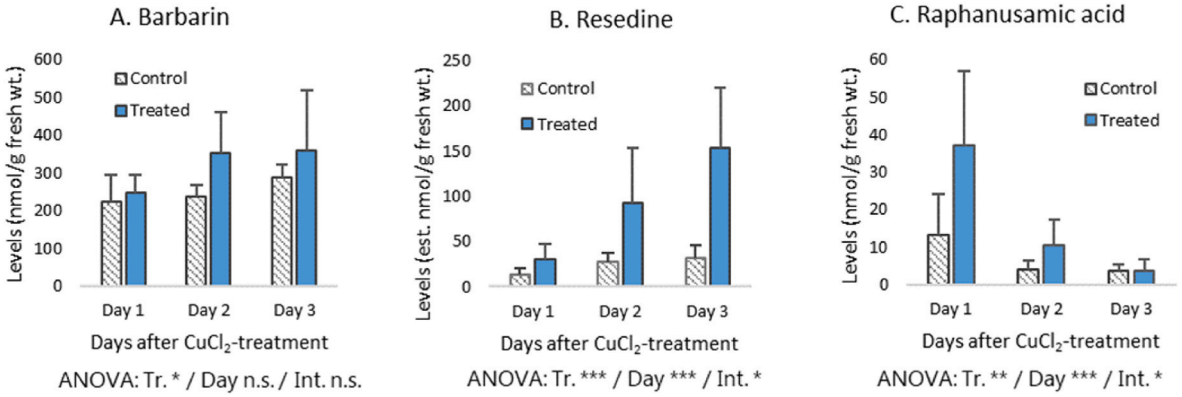


Fig. 9. Levels of selected glucosinolate hydrolysis products as a function of time in young rosette leaves after $CuCl_2$-treatment (treated) or mock treatment (control) of G-type *Barbarea vulgaris* plants. The hydrolysis products considered are (A) barbarin, (B) resedine, and (C) raphanusamic acid. Bars depict means, whiskers indicate standard deviations.

biosynthetic genes of GSL-derived phytoalexins is still in its infancy (Klein and Sattely, 2017). Hence, the focus of the present investigation was to characterize profile, time course and metabolic interactions of cyclonasturlexin (**P3**) and nasturlexin D (**P6**) biosynthesis in the genetically most well characterized system containing these promising phytoalexins: *B. vulgaris*. Based on previously reported sequences of enzymes in the biosynthesis of brassinin (**P1**) and **P2**, we searched the G-type genome for homologs and previously identified homologs of the atypical myrosinase candidate *Br*BABG (Agerbirk et al., 2018). We have now further identified homologs of the dithiocarbamate methyl transferases *Br*DTC-MT a and b, and the **P1** to **P2**-converting BrCYP71CR 1 and 2 (manuscript in preparation). These identifications suggested to us that *B. vulgaris* could be a suitable experimental system for investigating the biosynthesis of indole phytoalexin **P3** and phenyl containing phytoalexins such as **P6**. Such investigations would complement the investigations of **P1** and **P2** biosynthesis in *B. rapa* (Klein and Sattely, 2017). Although myrosinase activity in *Barbarea vulgaris* upon tissue disruption is well-established (e.g. Agerbirk and Olsen, 2015; Müller et al., 2018) and sequences of several candidate genes have been reported (Liu et al., 2016), the gene(s) and enzyme(s) have apparently not been named and characterized phylogenetically. For this reason, the general abbreviation MYR is used here (Figs. 1, Fig. 2, Fig. 3). Classifying myrosinases in *B. vulgaris* and unraveling their roles in general GSL hydrolysis and biosynthesis of two distinct groups of phytoalexins is obviously a future priority.

Identifying the site of phytoalexin biosynthesis is crucial for the planning of biosynthetic investigations. Our results suggest (terminal lobes of) rosette leaves, but not roots, to be a site of phytoalexin biosynthesis after foliar abiotic elicitation, based on detection of phytoalexins in leaves but barely in roots, and detection of a plausible metabolic signature in leaves. However, phytoalexin biosynthesis in general can happen in roots (Koprivova et al., 2023), possibly also in *B. vulgaris*. Phytoalexin biosynthesis may be part of a hypersensitive response; this would suggest *in situ* biosynthesis. However, GSL levels are not uniform in leaves; patterns of distribution have been reported (Schroff et al., 2008). Indeed, complex transport processes and non-uniform patterns of gene expression seem to be involved in creating the patterns of GSL distribution (Madsen et al., 2014; Sønderby et al., 2010; Nintemann et al., 2018). Petioles or other basal rosette parts could have a role in phytoalexin biosynthesis in analogy with the prominent part in GSL biosynthesis played by the vascular system and basal leaf parts. These hypotheses could be tested by MS imaging (Lorensen et al., 2023; Maia et al., 2022) and visual reporter genes based on genes presumably involved in phytoalexin biosynthesis, e.g. the atypical myrosinases and methyl transferases. Comparable investigation of camalexin biosynthesis in *A. thaliana* showed the biosynthesis to be restricted to the necrotic spots due to the eliciting pathogen (Schuhegger et al., 2007).

Although strong fluctuations in 4-substituted indole GSLs were observed after phytoalexin-elicitation in some experiments, the reproducibility was poor. These indole GSLs are biosynthesized from IM (Pfalz et al., 2011). Marked increase in a 4-substituted indole GSL was also reported upon $CuCl_2$ treatment (Pedras et al., 2008) or pathogen exposure (Aghajanzadeh et al., 2023) of *B. rapa*. Levels of the parent indole GSL IM were more stable in our investigation, although IM is the biosynthetic precursor of the indole phytoalexins **P1**–**P3**. However, due to the considerable levels of IM, even a substantial drain of the IM pool might not be distinguishable in metabolic analyses.

From tracer experiments in a related species, *B. verna* (Pedras and To, 2018), two potential GSL precursors of phenyl-containing phytoalexins had been suggested, PE and its *m*-hydroxy derivative 3hPE (Fig. 2). Levels of PE were consistently reduced after $CuCl_2$ treatment compared to mock treatment. We interpret this result as consistent with nasturlexin D (**P6**) biosynthesis from PE, happening in the analyzed leaves. The additional potential precursor, 3hPE, was not detectable during the period of **P6** accumulation. PE is one of the most widespread GSLs in crucifers (Bell and Wagstaff, 2017; Agerbirk et al., 2021a), including cruciferous crops such as radish (Shang et al., 2022) and oilseed rape (Missinou et al., 2022). The biosynthesis of PE is also well-understood (Liu et al., 2016; Wang et al., 2021). Hence, biotechnological (Poveda et al., 2020) or classical genetic introduction of nasturlexin D (**P6**) biosynthesis starting from PE would potentially be feasible for several cruciferous crops.

The parallel accumulation of barbarin and resedine is evidence for general GSL hydrolysis coinciding with the elicitation of phytoalexins, but whether this general GSL hydrolysis is mechanistically linked to phytoalexin biosynthesis or rather a mechanistically independent effect of the $CuCl_2$ treatment cannot be concluded. An independent effect could involve two different myrosinases, one of which could be BABG (Fig. 2), acting independently on PE and glucobarbarins, respectively. The association of resedine with phytoalexin accumulation tended to be stronger than the association of barbarin with phytoalexins, in agreement with an enzyme ("oxazolidinethionase") (Agerbirk et al., 2018) converting barbarin to resedine during phytoalexin biosynthesis. This enzyme is among several recently reported pathways in GSL turnover (Sugiyama et al., 2021; Andernach et al., 2023), and the association of resedine with phytoalexin accumulation suggest that oxazolidinethionase is part of a response to infection and could be studied in $CuCl_2$--treated plants. The rapid decline of raphanusamic acid levels would likewise suggest turnover of this early detoxification product of free isothiocyanates (Jeschke et al., 2019; Sugiyama et al., 2021). In contrast, resedine accumulated; whether resedine is eventually turned over is yet unclear.

The observation of accumulating products of phenyl-containing GSLs yet essentially stable levels of this group of GSLs is not surprising given the actual levels observed: even the highest levels of barbarin and resedine combined were less than one μmol/g, while total GSL levels were on average between five and ten μmol/g. Hence, the biochemical conditions of $CuCl_2$-treated leaves were far from those of physically disintegrated leaves, in which the entire pool of GSLs is rapidly hydrolysed (Agerbirk and Olsen, 2015). Furthermore, levels of GSLs represent a balance between biosynthesis and turnover, and in another case of leaf stress (herbivory), biosynthesis of *B. vulgaris* GSLs was indeed induced (Liu et al., 2016). *De novo* IM biosynthesis was also responsible for an IM-derived response to pathogen challenge *A. thaliana* (Hunziger et al., 2020). Overall, rosette leaves would represent a suitable plant part for future detailed investigations of the dynamics of GSL biosynthesis and turnover that occurs in parallel to or as part of biosynthesis of nasturlexin D (**P6**).

Flavonoids have so far been little investigated in G- and P-types of *B. vulgaris*, although four structures are known from the G-type (Dalby-Brown et al., 2011) and genetic loci responsible for tetraglycosylated flavonoids had been genetically mapped from a G-type/P-type F2 population (Kuzina et al., 2011). Presence of all four previously reported G-type flavonoids were confirmed for the G-type plants investigated here. Since levels of the dominant identified flavonoid **F1** in G-type plants were not dependent of the $CuCl_2$-treatment according to ANOVA or related to phytoalexin levels in a linear model, we concluded that there were no signs of a disturbance of flavonoid metabolism from the elicitation of phytoalexins using 10 mM $CuCl_2$. A similar experiment was reported from experiments with a crop, *B. rapa* (Pedras et al., 2008). In that case, levels of four flavonoids were unaffected or moderately increased by $CuCl_2$ treatment. In somewhat contrast to our hypothesis of independence between phytoalexin elicitation and flavonoids, a recent paper reported metabolic cross talk between GSLs and flavonoids (Tian et al., 2023).

In conclusion, we have identified genotypes, conditions and plant parts that should allow future molecular investigations of the biosynthesis of three agronomically promising phytoalexins in *B. vulgaris*. This biochemical system adds to the potentially useful genes of this popular eco-model plant, stressing the relevance of continued development of a comprehensive toolbox for genetic, chemical and molecular biological

investigations of this natural genetic resource (Nielsen et al., 2010; Van Molken et al., 2014a, 2014b; Christensen et al., 2019; Hauser et al., 2021). Indeed, the insect deterrent saponins of *B. vulgaris* are unique among crucifers, and the structurally remarkable indole phytoalexin cyclonasturlexin (**P3**) and phenyl-containing nasturlexin D (**P6**) are confined to a narrow group of cruciferous species. In general, the remarkable chemical profiles of *B. vulgaris* and *N. officinale* confirms the general value of screening wild species and non-model systems (e.g. Pedras et al., 2011; Pedras and Alavi, 2020; Zhou and Jander, 2021) as a supplement to the investigation of the usual model systems for insect and disease resistance mechanisms.

4. Experimental

4.1. General

Authentic standards of the phytoalexins brassinin (**P1**), cyclobrassinin (**P2**), cyclonasturlexin (**P3**), nasturlexin A (**P4**), nasturlexin C (**P5**), nasturlexin D (**P6**), nasturlexin B (**P9**) and tridentatol C (**P10**) were received as a gift in Jan. 2017 from Professor M.S.C. Pedras, University of Saskatchewan (Pedras and To, 2015, 2016; Pedras et al., 2015). Authentic standards of desulfoGSLs (desulfated derivatives of PE, 3hPE, 4hPE, BAR, EBAR, 4hBAR, 4hEBAR, 3hBAR, 3moBZ, 4moBZ, IM, 4hIM, 4moIM, 1moIM) were prepared as previously described (Agerbirk et al., 2015, 2021b, 2022). Authentic standards of GSL hydrolysis products and some downstream products were isolated as previously reported for barbarin, kjaerin and *m*-hydroxybarbarin (Agerbirk and Olsen, 2015), and resedine (Agerbirk et al., 2018). Authentic standards of *B. vulgaris* G-type flavonoids **F1**, **F2**, **F3** and **F4** were obtained as previously described (Dalby-Brown et al., 2011). The flavonoid rutin (R9000) (quercetin 3-*O*-(6-*O*-*α*-L-rhamnopyranosyl)-*β*-D-glucopyranoside) was from Sigma (now Sigma-Aldrich, St. Louis, MO). Raphanusamic acid was from Sigma-Aldrich (St. Louis, MO). BenzylGSL (K^+ salt) was from Merck (Darmstadt, Germany). For elicitation of phytoalexin biosynthesis in plants, $CuCl_2$ dihydrate (>99.99%) was from Aldrich (now Sigma-Aldrich, St. Louis, MO). Solvents for both extraction and LC were HPLC grade (including water of milliQ quality for the elicitation solution, solvents and LC). Data were managed in Microsoft Excel (2016), and general statistical operations (e.g. ANOVA, linear regression analysis) were carried out using the Analysis ToolPak Add-in for Excel. ANOVA for one set of data with different numbers of observations after removal of an outlier was incompatible with the Excel add-in and carried out using R Studio v. 2022.02.3. Statistical testing of correlation or regression was only carried out based on rational hypotheses or for testing previously reported correlations; all statistical tests carried out are reported. As a control for possible false positives due to multiple testing, we took into account two or three independent experiments (Table 2).

4.2. Plant material, cultivation and elicitation

Seeds of the G-type of *Barbarea vulgaris* were generally of accession B44 (NGB 31789) while seeds of the P-type of the same species were of accession B4 (NGB 23547) (Agerbirk et al., 2021b). Both accessions are available from https://nordic-baltic-genebanks.org, registered under the indicated NGB numbers. However, for experiment 1 ("leaf position experiment"), two other G-type and two other P-type accessions were used as detailed elsewhere (Agerbirk et al., 2022). Both accessions agree with descriptions of ssp. *arcuata* (Opiz.) Fries in standard floras (e.g. Hegi, 1958), but are currently not named to subspecies level due to their contrasting phylogeny (Lange et al., 2022).

Plants were sown and grown in a standard, peat based artificial soil and cultivated in a heated greenhouse (typically around 20 °C) with supplemental light (16 h L: 8 h D) and standard complete mineral fertilizer applied (Azelis pioner basis NPK 13-2-23, Tanggaard, Bjæverskov, Denmark). Two weeks before elicitation experiments, individual rosette plantlets (3–4 weeks old, typically in the 4–6 true leaves stadium) were potted in individual pots (9 cm diameter, 7 cm height) and allowed liberal space (8 pots per tray of ca. 1500 cm^2) to develop optimally.

4.3. Elicitation experiments

The general conditions were used for elicitation experiments No. 2 and 3, which took place in the spring (exp. 2) and summer (exp. 3) 2019 in the Copenhagen University greenhouse facilities. The treatment consisted of spraying with either 10 mM $CuCl_2$ (*aq*) or water as control. For spraying, in order to avoid contamination of our general facilities with $CuCl_2$, both control and test plants were taken outdoor in mild weather, avoiding extremes of temperature or UV light. The plant to be sprayed was placed in a cardboard box open to one side, and sprayed with liberal amounts of the relevant solution both from below and above leaves using a simple plastic spray bottle obtained in a local supermarket (separate bottles for $CuCl_2$ (*aq*) and water). Surplus solution was allowed to drip off. Separate cardboard boxes were used for $CuCl_2$ (*aq*) and water to avoid contamination, and physical contact across the treatment groups was avoided. After the elicitation, plants were returned to the greenhouse and placed in a block design for attempted uniform growth conditions within the plant types (G or P). For each plant type, two blocks in trays placed diagonally were used for test ($CuCl_2$) or control plants. For daily sampling in the following three days, plants were taken at random from both diagonally placed blocks. In experiments comparing the two plant types (G and P), a symmetrical design to randomize the conditions experienced by each plant type was not used, but the G-type blocks and P-type blocks were kept at apparently similar conditions along the center of the same green-house shelf and were treated and sampled in parallel on the same days.

Three biological experiments were carried out in 2017–2019. Experiment No. 1 ("leaf position experiment") in June 2017 investigated relative phytoalexin levels in a gradient of leaf positions in both P and G-type plants. The conditions differed somewhat from the general conditions (plants grown in a growth chamber, only leaves sampled, leaves dried over silica gel and stored frozen with silica gel until extraction). The four youngest fully developed or nearly fully developed rosette leaves were sampled from each rosette plant (Leaf 2–5), and only one sampling time was used; 2 days after elicitation, resulting in 20 P-type and 20 G-type treated leaf samples representing four leaf positions from 5 G-type and 5 P-type plants, and an equal number of control samples. GSL levels and lack of aliphatic GSLs from some of these leaves were reported elsewhere (Agerbirk et al., 2021b). For the present paper, we extracted all treated G-type leaves, leaves of three G-type controls and one P-type control, and the four leaf positions of one treated P-type plant in triplicate, using 10 mg dry leaf tissue for each extraction.

Experiment No. 2 ("P and G leaf elicitation experiment") in May 2019 was a 2 × 2 x 3 factor experiment with 3 biological replicates comparing two plant types (P and G) and two elicitation regimes (10 mM $CuCl_2$ (*aq*) or water) over 3 days (1, 2 or 3 after the treatment), resulting in 36 samples analyzed for phytoalexins and GSLs.

Experiment No. 3 ("G leaf versus root elicitation experiment") in August 2019 repeated the G-type half of experiment 2 but both leaves and roots of the G-type plants were sampled and the number of biological replicates set to 5 per treatment, resulting in $2 \times 2 \times 3 \times 5 = 60$ samples analyzed for phytoalexins and GSLs. One leaf GSL sample (Day 1 control #5) was dismissed as it exhibited clear signs of contamination with a root sample.

4.4. Extraction and preparation of extracts for metabolite analyses

A combined extraction of *B. vulgaris* leaves for both GSL and phytoalexin analysis were carried out as follows. For sampling leaves, only the terminal lobe of the selected rosette leaf was extracted. In experiments 2 and 3, we used the innermost fully or nearly fully developed rosette leaf. For sampling roots in experiment 3, peat around the entire root system

of the rosette plant was manually removed as well as possible, requiring around 1 min, and remaining peat rinsed of during a brief rinse with tap water followed by gently drying between tissue paper. Immediately before each extraction, the relevant plant part was picked and the fresh wt. (typically 0.2–0.7 g) was measured on an analytical balance in a beaker. Within ca. 1 min, extraction solvent, ca. 5 mL MeOH–H_2O (7:3), was brought to boiling on a hotplate and poured over the plant material in the beaker, and extraction was performed for 60 s, keeping the solvent boiling using the hotplate. The extract was poured into a volumetric flask (10.00 mL) and a second round of extraction was performed. The combined extracts were adjusted to 10.00 mL by addition of extraction solvent (or in a few cases by evaporation of surplus solvent under a gentle air stream). The combined extract was poured into a beaker with attention to complete mixing, and 4.50 mL was taken twice for determination of phytoalexins and GSLs (Section 4.6.), respectively. For phytoalexin determination, the solvent was evaporated under a gentle air-stream and the residue was dissolved and transferred quantitatively in 3 × 200 μL of MeOH–H_2O (1:2), centrifuged for 2 min at 20.000 g, filtered through a 0.22 μm filter (Merck Millipore, Cork, IRL) and subjected to UHPLC-analysis (Section 4.5.).

4.5. UHPLC-QToF MS of phytoalexins, glucosinolate hydrolysis products and flavonoids

Phytoalexins, GSL hydrolysis products and flavonoids were separated, identified and quantified by UHPLC-QToF MS, performed on a Dionex UltiMate 3000 Quaternary Rapid Separation UHPLC$^+$ focused system (Thermo Fisher Scientific, Germering, Germany). Injection volume was 10 μL. Separation was achieved on a Kinetex 1.7 μm XB-C18 column (100 × 2.1 mm, 1.7 μm, 100 Å, Phenomenex). For elution, 0.05% (v/v) formic acid in H_2O and acetonitrile [supplied with 0.05% (v/v) formic acid] were employed as mobile phases A and B, respectively. Gradient conditions were as follows: 0.0−0.5 min 10% B; 0.5−4.0 min 10−45% B, 4.0−10.5 min 45–75% B, 10.5−11.5 min 75–100% B, 11.5−12.5 min 100% B, 12.5−12.6 min 100−10% B, and 12.6−15.0 min 10% B. The flow rate of the mobile phase was 300 μL/min. The column temperature was maintained at 30 °C. UV absorbance chromatograms were additionally recorded at 229, 260, 310, and 345 nm. The UHPLC was coupled to a Compact micrOTOF-Q mass spectrometer (Bruker, Bremen, Germany) equipped with an electrospray ion source (ESI). The ion spray voltage was maintained at +4500 V in positive ion mode. Dry temperature was set to 250 °C, and the dry gas flow was set to 8 L/min. Nitrogen was used as the dry gas, nebulizing gas, and collision gas. The nebulizing gas was set to 2.5 bar and collision energy to 10 eV in positive ion mode. MS spectra were acquired in an *m/z* range from 50 to 1000 and MS/MS spectra in a range from 100 to 800. Sampling rate was 2 Hz. Na-formate clusters were used for mass calibration. All files were automatically calibrated by postprocessing. Chiral UHPLC-QToF MS of kjaerin was carried out using different conditions as previously reported (Müller et al., 2018).

Quantification was based on external calibration curves. Received synthetic phytoalexins were stored over silica gel, weighed (ca. 0.3–1.8 mg) using a 5 decimal analytical scale (MC 210 S, Sartorius, Göttingen, Germany), each dissolved in 250 μl 80% aq. MeOH and diluted to 100 μM stocks in 30% aq. MeOH (assuming 100% purity) used to prepare pure dilutions in the analytical range as well as mixtures, from which factor 2 dilution series were made from 10.0 μM to 9.8 nM (Table 1). Serially diluted standards for rutin and **F1** were made similarly except that a factor 3 dilution curve was used (rutin) or an equidistant curve was made in the relevant concentration range (**F1**) (Figs. S3F–G). Standards of raphanusamic acid were made in eight concentrations between 125 nM and 100 μM (Figs. S2H–I). Standards of GSL products were as previously reported (Agerbirk and Olsen, 2015; Agerbirk et al., 2018), based on $\varepsilon_{245} = 1.9 \bullet 10^4$ $M^{-1}cm^{-1}$ for barbarin (Kjær and Gmelin, 1957). For peak recognition and integration, the automatic integration tool in Bruker Compass Data Analysis and the calibration curves (Table 1) were used. For quantification of analytes (in samples as well as unknowns), we created extracted ion chromatograms for the calculated monoisotopic mass of proton adducts using stringent conditions: ± 0.005 Da for metabolites below 500 Da and ± 0.010 Da for metabolites with mass equal to or higher than 500 Da. Initial inspection of chromatogram shapes and peak areas supported the use of these stringency parameters; less stringent extracted ion chromatograms did not generally result in higher peak areas while more stringent parameters affected peak shape and area. Manual integration was used for distinct peaks that escaped recognition by the program. For peaks well established in the plant type, manual integration of apparent traces or noise at the correct retention time was carried out for statistical reasons even if presence of the analyte was uncertain; the corresponding results served as maximum estimates.

4.6. Glucosinolate analysis using desulfation and UHPLC-QToF MS analysis

For GSL determination, the crude extract was stored frozen at −20 °C, then thawed and applied to an enzymatic on-column procedure for GSL desulfation followed by UHPLC-DAD-QToF MS analysis of the resulting desulfoGSLs, both exactly as described elsewhere (Agerbirk et al., 2022). For logistic reasons, the conversion to desulfoGSLs had to be carried out during three separate days; samples from all treatment groups as well as blanks and external standards were distributed symmetrically over the three days. Linearity testing showed linearity of the UV detector up to at least 6 mM of desulfoGSL, which was well above even major GSL peaks in the samples. However, linearity using the MS detector was much more limited, but extending up to ca. 10 μM in samples. This range allowed determination of minor GSLs such as PE and 4moIM from extracted ion chromatogram traces, while all major GSLs had to be determined from the UV peak areas measured at λ = 229 nm. For the peaks quantified from UV peak areas, levels were calculated from comparison with a reference of 0.535 μmol benzylGSL subjected to the desulfation procedure (corresponding to 0.9 mM desulfo benzylGSL in injected samples). For the peaks quantified from extracted ion chromatogram peak areas, levels were calculated from comparison with a reference of 8.0 μM desulfo BAR. From integration of minor peaks, the LOD was estimated as < 0.1 nmol/g fresh wt.

Author contributions

Conceived study idea: NA. Designed study: NA, PDC, JPL, SHL, NL, SW, KRJ, SB, CC. Performed biological experiments, extractions, sample prep.: PDC, JPL, SHL, NL, SW, KRJ, NA. Optimized LC-MS: DIP, CC, NA. Carried out LC-MS and instrument care: DIP, CC. LC-MS data analysis: NA, PDC, JPL, SHL, NL, SW, CC, DIP. Statistics and data analysis: NA, PDC, JPL, SHL, NL, SW, MB. Supervision: NA, PDC, SB, CC, MB. Interpretation and discussions: all. Manuscript draft: NA. Edits: All.

Declaration of competing interest

The authors declare that they have no known competing financial interests or personal relationships that could have appeared to influence the work reported in this paper.

Data availability

Data will be made available on request.

Acknowledgements

We thank Prof. M.S.C. Pedras for generously sharing standards and suggestions, including detailed comments to earlier versions of the manuscript, MSc E. Ciepiel for assisting with biological experiments, Dr. T. Yang for carrying out chiral HPLC of kjaerin, Dr. T.P. Hauser for

constructive discussions, Torben og Alice Frimodts Fond for financial support, and three anonymous reviewers for constructive comments which improved the manuscript.

Appendix A. Supplementary data

Supplementary data to this article can be found online at https://doi.org/10.1016/j.phytochem.2023.113742.

References

Agerbirk, N., Olsen, C.E., 2015. Glucosinolate hydrolysis products in the crucifer *Barbarea vulgaris* include a thiazolidine-2-one from a specific phenolic isomer as well as oxazolidine-2-thiones. Phytochemistry 115, 143–151. https://doi.org/10.1016/j.phytochem.2014.11.002.

Agerbirk, N., Olsen, C.E., Heimes, C., Christensen, S., Bak, S., Hauser, T., 2015. Multiple hydroxyphenethyl glucosinolate isomers and their tandem mass spectrometric distinction in a geographically structured polymorphism in the crucifer *Barbarea vulgaris*. Phytochemistry 115, 130–142. https://doi.org/10.1016/j.phytochem.2014.09.003.

Agerbirk, N., Matthes, A., Erthmann, P.Ø., Ugolini, L., Cinti, S., Lazaridi, E., Nuzillard, J.-M., Müller, C., Bak, S., Rollin, P., Lazzeri, L., 2018. Glucosinolate turnover in Brassicales species to an oxazolidin-2-one, formed via the 2-thione and without formation of thioamide. Phytochemistry 153, 79–83. https://doi.org/10.1016/j.phytochem.2018.05.006.

Agerbirk, N., Hansen, C.C., Kiefer, C., Hauser, T.P., Ørgaard, M., Lange, C.B.A., Cipollini, D., Koch, M.A., 2021a. Comparison of glucosinolate diversity in the crucifer tribe Cardamineae and the remaining order Brassicales highlights repetitive evolutionary loss and gain of biosynthetic steps. Phytochemistry 185, 112668. https://doi.org/10.1016/j.phytochem.2021.112668.

Agerbirk, N., Hansen, C.C., Olsen, C.E., Kiefer, C., Hauser, T.P., Christensen, S., Jensen, K.R., Ørgaard, M., Pattison, D.I., Lange, C.B.A., Cipollini, D., Koch, M.A., 2021b. Glucosinolate profiles and phylogeny in *Barbarea* compared to other tribe Cardamineae (Brassicaceae) and *Reseda* (Resedaceae), based on a library of ion trap HPLC-MS/MS data of reference desulfoglucosinolates. Phytochemistry 185, 112658. https://doi.org/10.1016/j.phytochem.2021.112658.

Agerbirk, N., Pattison, D.L., Mandákova, T., Lysak, M.A., Montaut, S., Staerk, D., 2022. Ancient biosynthesis in an oil crop: glucosinolate profiles in *Limnanthes alba* and its relatives (Limnanthaceae, Brassicales). J. Agric. Food Chem. 70, 1134–1147. https://doi.org/10.1021/acs.jafc.1c07299.

Aghajanzadeh, T., Watanabe, M., Tohge, T., Hawkesford, M.J., Fernie, A., Hoefgen, A.R., Elzenga, J.T.M., De Kok, L.J., 2023. Necrotrophic fungal infection affects indolic glucosinolate metabolism in *Brassica rapa*. Acta Physiol. Plant. 45, 64. https://doi.org/10.1007/s11738-023-03546-3.

Ahmed, S., Kovinich, N., 2021. Regulation of phytoalexin biosynthesis for agriculture and human health. Phytochemistry Rev. 20, 483–505. https://doi.org/10.1007/s11101-020-09691-8.

Ahuja, I., Kissen, R., Bones, A.M., 2012. Phytoalexins in defense against pathogens. Trends Plant Sci. 17, 73–90. https://doi.org/10.1016/j.tplants.2011.11.002.

Andernach, L., Witzel, K., Hanschen, F.S., 2023. Glucosinolate-derived amine formation in *Brassica oleracea* vegetables. Food Chem. 405, 134907 https://doi.org/10.1016/j.foodchem.2022.134907.

Barco, B., Clay, N.K., 2019. Evolution of glucosinolate diversity via whole-genome duplications, gene rearrangements, and substrate promiscuity. Annu. Rev. Plant Biol. 70, 585–604. https://doi.org/10.1146/annurev-arplant-050718-100152.

Bell, L., Wagstaff, C., 2017. Enhancement of glucosinolate and isothiocyanate profiles in Brassicaceae crops: addressing challenges in breeding for cultivation, storage and consumer-related traits. J. Agric. Food Chem. 65, 9379–9403. https://doi.org/10.1021/acs.jafc.7b03628.

Bhat, R., Vyas, D., 2019. Myrosinase: insights on structural, catalytic, regulatory, and environmental interactions. Crit. Rev. Biotechnol. 39 (4), 508–523. https://doi.org/10.1080/07388551.2019.1576024.

Blažević, I., Montaut, S., Burčul, F., Olsen, C.E., Burow, M., Rollin, P., Agerbirk, N., 2020. Glucosinolate structural diversity, identification, chemical synthesis and metabolism in plants. Phytochemistry 168, 112100. https://doi.org/10.1016/j.phytochem.2019.112100.

Byrne, S., Erthmann, P.Ø., Agerbirk, N., Bak, S., Hauser, T.P., Nagy, I., Paina, C., Asp, T., 2017. The genome sequence of *Barbarea vulgaris* facilitates the study of ecological biochemistry. Sci. Rep. 7, 40728 https://doi.org/10.1038/srep40728.

Christensen, S., Enge, S., Jensen, K.R., Müller, C., Kiær, L.P., Agerbirk, N., Heimes, C., Hauser, T.P., 2019. Different herbivore responses to two co-occurring chemotypes of the wild crucifer *B. vulgaris*. Arthropod Plant Inte 13, 19–30. https://doi.org/10.1007/s11829-018-9633-x.

Dalby-Brown, L., Olsen, C.E., Nielsen, J.K., Agerbirk, N., 2011. Polymorphism for novel tetraglycosylated flavonols in an eco-model crucifer, *Barbarea vulgaris*. J. Agric. Food Chem. 59, 6947–6956. https://doi.org/10.1021/jf200412c.

Erthmann, P.Ø., Agerbirk, N., Bak, S., 2018. A tandem array of UDP-glycosyltransferases from the UGT73C subfamily glycosylate sapogenins, forming a spectrum of mono- and bisdesmosidic saponins. Plant Mol. Biol. 97, 37–55. https://doi.org/10.1007/s11103-018-0723-z.

Günther, J., Erthmann, P.Ø., Khakimov, B., Bak, S., 2022. Reciprocal mutations of two multifunctional β-amyrin synthases from *Barbarea vulgaris* shift α/β-amyrin ratios. Plant Physiol. 188, 1483–1495. https://doi.org/10.1093/plphys/kiab545.

Halkier, B.A., 2016. General introduction to glucosinolates. Adv. Bot. Res. 80, 1–14. https://doi.org/10.1016/bs.abr.2016.07.001.

Hauser, T.P., Christensen, S., Kuzina, V., Thines, M., Ploch, S., Bak, S., 2021. Effects of a saponin-based insect resistance and a systemic pathogen resistance on field performance of the wild crucifer *Barbarea vulgaris*. Arthropod Plant Inte 15, 683–698. https://doi.org/10.1007/s11829-021-09858-w.

Hegi, G., 1958. Illustrierte Flora von Mittel-Europa. Carl Hanser Verlag, Münich, Germany.

Hunziger, P., Ghareeb, H., Wagenknecht, L., Crocoll, C., Halkier, B.A., Lipka, V., Schulz, A., 2020. De novo indol-3-ylmethyl glucosinolate biosynthesis, and not long-distance transport, contributes to defence of Arabidopsis against powdery mildew. Plant Cell Environ. 1–13. https://doi.org/10.1111/pce.13766.

Jeschke, V., Weber, K., Moore, S.S., Burow, M., 2019. Coordination of glucosinolate biosynthesis and turnover under different nutrient conditions. Front. Plant Sci. 10, 1560. https://doi.org/10.3389/fpls.2019.01560.

Kariya, K., Fujita, A., Ueno, M., Yoshikawa, T., Teraishi, M., Taniguchi, Y., Ueno, K., Ishihara, A., 2023. Natural variation of diterpenoid phytoalexins in rice: aromatic diterpenoid phytoalexins in specific cultivars. Phytochemistry 211, 113708. https://doi.org/10.1016/j.phytochem.2023.113708.

Kjær, A., Gmelin, R., 1957. *Iso*thiocyanates XXVIII. A new *iso*thiocyanate glucoside (glucobarbarin) furnishing (-)-5-phenyl-2-oxazolidinethione upon enzymatic hydrolysis. Acta Chem. Scand. 11, 906–907. https://doi.org/10.3891/acta.chem.scand.11-0906.

Klein, A.P., Sattely, E.S., 2015. Two cytochromes P450 catalyze *S*-heterocyclizations in cabbage phytoalexin biosynthesis. Nat. Chem. Biol. 11, 837–839. https://doi.org/10.1038/NCHEMBIO.1914.

Klein, A.P., Sattely, E.S., 2017. Biosynthesis of cabbage phytoalexins from indole glucosinolates. Proc. Natl. Acad. Sci. U.S.A. 114, 1910–1915. https://doi.org/10.1073/pnas.1615625114.

Koprivova, A., Schwier, M., Volz, V., Kopriva, S., 2023. Shoot-root interaction in control of camalexin exudation in Arabidopsis. J. Exp. Bot. 74, 2667–2679. https://doi.org/10.1093/jxb/erad031.

Kuzina, V., Nielsen, J.K., Augustin, J.M., Torp, A.M., Bak, S., Andersen, S.B., 2011. *Barbarea vulgaris* linkage map and quantitative trait loci for saponins, glucosinolates, hairiness and resistance to the herbivore *Phyllotreta nemorum*. Phytochemistry 72, 188–198. https://doi.org/10.1016/j.phytochem.2010.11.007.

Lange, C.B.A., Hauser, T.P., Deichmann, V., Ørgaard, M., 2022. Hybridization and complex evolution of *Barbarea vulgaris* and related species (Brassicaceae). Mol. Phylogenet. Evol. 169, 107425 https://doi.org/10.1016/j.ympev.2022.107425.

Liu, T., Zhang, X., Yang, H., Agerbirk, N., Qiu, Y., Wang, H., Shen, D., Song, J., Li, X., 2016. Aromatic glucosinolate biosynthesis pathway in *Barbarea vulgaris* and its response to *Plutella xylostella* infestation. Front. Plant Sci. 7, 83. https://doi.org/10.3389/fpls.2016.00083.

Liu, T.-J., Zhang, Y.-J., Agerbirk, N., Wang, H.-P., Wei, X.-C., Song, J.-P., He, H.-J., Zhao, X.-Z., Zhang, X.-H., Li, X.-X., 2019a. A high-density genetic map and QTL mapping of leaf traits and glucosinolates in *Barbarea vulgaris*. BMC Genom. 20, 371. https://doi.org/10.1186/s12864-019-5769-z.

Liu, T., Khakimov, B., Cardenas, P.D., Cozzi, F., Olsen, C.E., Jensen, K.R., Hauser, T.P., Bak, S., 2019b. The cytochrome P450 CYP72A552 is key to production of hederagenin-based saponins that mediate plant defense against herbivores. New Phytol. 222, 1599–1609. https://doi.org/10.1111/nph.15689.

Lorensen, M.D.B.B., Bjarnholt, N., St-Pierre, B., Heinicke, S., Courdavault, V., O'Connor, S., Janfelt, C., 2023. Spatial localization of monoterpenoid indole alkaloids in Rauvolfia tetraphylla by high resolution mass spectrometry imaging. Phytochemistry 209, 113620. https://doi.org/10.1016/j.phytochem.2023.113620.

Lv, Q., Li, X., Fan, B., Zhu, C., Chen, Z., 2022. The cellular and subcellular organization of the glucosinolate–myrosinase system against herbivores and pathogens. Int. J. Mol. Sci. 23, 1577. https://doi.org/10.3390/ijms23031577.

Madsen, S.R., Olsen, C.E., Nour-Eldin, H.H., Halkier, B.A., 2014. Elucidating the role of transport processes in leaf glucosinolate distribution. Plant Physiol. 166, 1450–1462. https://doi.org/10.1104/pp.114.246249.

Maia, M., Carré, V., Aziz, A., Jeandet, P., 2022. Molecular localization of phytoalexins at the micron scale: toward a better understanding of plant-phytoalexin-pathogen dynamics. J. Agric. Food Chem. 70, 9243–9245. https://doi.org/10.1021/acs.jafc.2c04208.

Malhotra, B., Kumar, P., Bisht, N.C., 2022. Defense versus growth trade-offs: insights from glucosinolates and their metabolites. Plant Cell Environ. https://doi.org/10.1111/pce.14462.

Missinou, A.A., de Carvalho, J.F., Marnet, N., Delhaye, T., Hamzaoui, O., Sayed, D.A., Guitton, Y., Lebreton, L., Langrume, C., Laperche, A., Delourme, R., Manzanares-Dauleux, M.J., Bouchereau, A., Gravot, A., 2022. Identification and quantification of glucosinolates and phenolics in a large panel of *Brassica napus* highlight valuable genetic resources for chemical ecology and breeding. J. Agric. Food Chem. 70, 5245–5261. https://doi.org/10.1021/acs.jafc.1c08118.

Monde, K., Takasugi, M., Ohnishi, T., 1994. Biosynthesis of cruciferous phytoalexins. J. Am. Chem. Soc. 116, 6650–6657. https://doi.org/10.1021/ja00094a021.

Møldrup, M.E., Salomonsen, B., Geu-Flores, F., Olsen, C.E., Halkier, B.A., 2013. *De novo* genetic engineering of the camalexin biosynthetic pathway. J. Biotechnol. 167, 296–301. https://doi.org/10.1016/j.jbiotec.2013.06.013.

Mucha, S., Heinzlmeir, S., Kriechbaumer, V., Strickland, B., Kirchhelle, C., Choudhary, M., Kowalski, N., Eichmann, R., Hückelhoven, R., Grill, E., Kuster, B., Glawischnig, E., 2019. The formation of a camelexin biosynthetic metabolon. Plant Cell 31, 2697–2710. https://doi.org/10.1105/tpc.19.00403.

Müller, C., Schulz, M., Pagnotta, E., Ugolini, L., Yang, T., Matthes, A., Lazzeri, L., Agerbirk, N., 2018. The role of the glucosinolate-myrosinase system in mediating

greater resistance of *Barbarea verna* than *B. vulgaris* to *Mamestra brassicae* larvae. J. Chem. Ecol. 44, 1190–1205. https://doi.org/10.1007/s10886-018-1016-3.
Nakano, R.T., Pislewska-Bednarek, M., Yamada, K., Edger, P.P., Miyahara, M., Kondo, M., Böttcher, C., Mori, M., Nishimura, M., Schulze-Lefert, P., Hara-Nishimura, I., Bednarek, P., 2017. PYK10 myrosinase reveals a functional coordination between endoplasmatic reticulum bodies and glucosinolates in *Arabidopsis thaliana*. Plant J. 89, 204–220. https://doi.org/10.1111/tpj.13377.
Nielsen, J.K., Nagao, T., Okabe, H., Shinoda, S., 2010. Resistance in the plant, *Barbarea vulgaris*, and counteradaptations in flea beetles mediated by saponins. J. Chem. Ecol. 36, 277–285. https://doi.org/10.1007/s10886-010-9758-6.
Nintemann, S.J., Hunziker, P., Andersen, T.G., Schulz, A., Burow, M., Halkier, B.A., 2018. Localization of the glucosinolate biosynthetic enzymes reveals distinct spatial patterns for the biosynthesis of indole and aliphatic glucosinolates. Physiol. Plantarum 163, 138–154. https://doi.org/10.1111/ppl.1267.
Pastorczyk, M., Bednarek, P., 2016. The function of glucosinolates and related metabolites in plant innate immunity. Adv. Bot. Res. 80, 171–197. https://doi.org/10.1016/bs.abr.2016.06.007.
Pedras, M.S.C., Zheng, Q.-A., Gadagi, R.S., Rimmer, S.R., 2008. Phytoalexins and polar metabolites from the oilseeds canola and rapeseed: differential metabolic responses to the biotroph *Albuga candida* and to abiotic stress. Phytochemistry 69, 894–910. https://doi.org/10.1016/j.phytochem.2007.10.019.
Pedras, M.S.C., Yaya, E.E., Glawischnig, E., 2011. The phytoalexins from cultivated and wild crucifers: chemistry and biology. Nat. Prod. Rep. 28, 1381–1405. https://doi.org/10.1039/c1np00020a.
Pedras, M.S.C., Yaya, E.E., 2013. Dissecting metabolic puzzles through isotope feeding: a novel amino acid in the biosynthetic pathway of the cruciferous phytoalexins rapalexin A and isocyalexin. A. Org. Biomol. Chem. 11, 1149–1166. https://doi.org/10.1039/c2ob27076e.
Pedras, M.S.C., 2014. Chemistry and biology of the cruciferous phytoalexins brassinin and cyclobrassinin. Nat. Prod. J. 4, 166–172. https://doi.org/10.2174/2210315504666141016222025.
Pedras, M.S.C., To, Q.H., 2015. The first non-indolyl cruciferous phytoalexins: nasturlexins and tridentatols, a striking convergent evolution of defenses in terrestrial plants and marine animals? Phytochemistry 113, 57–63. https://doi.org/10.1016/j.phytochem.2014.07.024.
Pedras, M.S.C., Alavi, M., To, Q.H., 2015. Expanding the nasturlexin family: nasturlexins C and D and their sulfoxides are phytoalexins of the crucifers *Barbarea vulgaris* and *B. verna*. Phytochemistry 118, 131–138. https://doi.org/10.1016/j.phytochem.2015.08.009.
Pedras, M.S.C., To, Q.H., 2016. Unveiling the first indole-fused thiazepine: structure, synthesis and biosynthesis of cyclonasturlexin, a remarkable cruciferous phytoalexin. Chem. Commun. 52, 5880–5883. https://doi.org/10.1039/c6cc02108e.
Pedras, M.S.C., Abdoli, A., 2017. Pathogen inactivation of cruciferous phytoalexins: detoxification reactions, enzymes and inhibitors. RSC Adv. 7, 23633–23646. https://doi.org/10.1039/c7ra01574gzaki.
Pedras, M.S.C., To, Q.H., 2018. Interrogation of biosynthetic pathways of the cruciferous phytoalexins nasturlexins with isotopically labelled compounds. Org. Biomol. Chem. 16, 3625–3638. https://doi.org/10.1039/C8OB00673C.
Pedras, M.S.C., Alavi, M., 2020. Expanding the phytoalexin chemical space: tropalexins A and B from *Tropaeolum majus* suggest evolutionary conservation of biosynthetic enzymes. Chem. https://doi.org/10.26434/chemrxiv.13350335.v1.
Pfalz, M., Mikkelsen, M.D., Bednarek, P., Olsen, C.E., Halkier, B.A., Kroymann, J., 2011. Metabolic engineering in *Nicotiana benthamiana* reveals key enzyme functions in *Arabidopsis thaliana* indole glucosinolate modification. Plant Cell 23, 716–729. https://doi.org/10.1105/tpc.110.081711.
Plaszkó, T., Szücs, Z., Vasas, G., Gonda, S., 2022. Interactions of fungi with non-isothiocyanate products of the plant glucosinolate pathway: a review on product formation, antifungal activity, mode of action and biotransformation. Phytochemistry 200, 113245. https://doi.org/10.1016/j.phytochem.2022.113245.
Poveda, J., Francisco, M., Cartea, M.E., Velasco, P., 2020. Development of transgenic *Brassica* crops against biotic stresses caused by pathogens and arthropod pests. Plants 9, 1664. https://doi.org/10.3390/plants9121664.
Schroff, R., Muck, A., Gershenzon, J., 2008. Nonuniform distribution of glucosinolates in *Arabidopsis thaliana* leaves has important consequences for plant defense. Proc. Nat. Acad. Sci. USA 105, 6196–6201. https://doi.org/10.1073/pnas.0711730105.
Schuhegger, R., Rauhut, T., Glawischnig, E., 2007. Regulatory variability of camalexin biosynthesis. J. Plant Physiol. 164, 636–644. https://doi.org/10.1016/j.jplph.2006.04.012.
Shang, G., Zhao, H., Tong, L., Yin, N., Hu, R., Jiang, H., Kamal, F., Zhao, Z., Xu, L., Lu, K., Li, J., Qu, C., Du, D., 2022. Genome-wide association study of phenylalanine derived glucosinolates in Brassica rapa. Plants 11, 1274. https://doi.org/10.3390/plants11091274.
Sønderby, I.E., Burow, M., Rowe, H.C., Kliebenstein, D.J., Halkier, B.A., 2010. A complex interplay of three R2R3 MYB transcription factors determines the profile of aliphatic glucosinolates in Arabidopsis. Plant Physiol. 153, 348–363. https://doi.org/10.1104/pp.109.149286.
Sugiyama, R., Li, R., Kuwahara, A., Nakabayashi, R., Sotta, N., Mori, T., Ito, T., Ohkama-Ohtsu, N., Fujiwara, T., Saito, K., Nakano, R.T., Bednarek, P., Hirai, M.Y., 2021. Retrograde sulfur flow from glucosinolates to cysteine in *Arabidopsis thaliana*. Proc. Natl. Acad. Sci. U.S.A. 118, 22. https://doi.org/10.1073/pnas.2017890118.
Tian, X., He, H., Yu, X., Wang, Y., Hu, L., Cheng, B., Ding, Y., Liu, G., 2023. Transcriptome and metabolome analyses of glucosinolate biosynthesis-related genes in different organs of broccoli (*Brassica oleracea* L. var. *italica*). Appl. Sci. 13, 5837. https://doi.org/10.3390/app13105837.
Van Molken, T., Heimes, C., Hauser, T.P., Sundelin, T., 2014a. Phylogeny of an *Albugo* sp. infecting *Barbarea vulgaris* in Denmark and its frequency of symptom development in natural populations of two evolutionary divergent plant types. Fungal Biol 118, 340–347. https://doi.org/10.1016/j.funbio.2014.01.008.
Van Molken, T., Kuzina, V., Munk, K.R., Olsen, C.E., Sundelin, T., van Dam, N.M., Hauser, T.P., 2014b. Conequences of combined herbivore feeding and pathogen infection for fitness of *Barbarea vulgaris* plants. Oecologia 175, 589–600. https://doi.org/10.1007/s00442-014-2928-4.
VanEtten, H.D., Mansfield, J.W., Bailey, J.A., Farmer, E.E., 1994. Two classes of plant antibiotics: "Phytoalexins" versus "phytoanticipins.". Plant Cell 6, 1191–1192.
Wang, C., Dissing, M.M., Agerbirk, N., Crocoll, C., Halkier, B.A., 2021. Engineering and optimization of the 2-phenylethylglucosinolate production in *Nicotiana benthamiana* by combining biosynthetic genes from *Barbarea vulgaris* and *Arabidopsis thaliana*. Plant J. 106, 978–992. https://doi.org/10.1111/tpj.15212.
Yamada, K., Goto-Yamada, S., Nakazaki, A., Kunieda, T., Kuwata, K., Nagano, A.J., Nishimura, M., Hara-Nishimura, I., 2020. Endoplasmic reticulum-derived bodies enable a single-cell chemical defense in Brassicaceae plants. Commun. Biol. 3, 21. https://doi.org/10.1038/s42003-019-0739-1.
Zhou, S., Jander, G., 2021. Engineering insect resistance using plant specialized metabolites. Curr. Opin. Biotechnol. 70, 115–121. https://doi.org/10.1016/j.copbio.2021.03.005.